Published in final edited form as:
J Comp Neurol. 2008 June 20; 508(6): 906–926. doi:10.1002/cne.21684.

Cytology and Receptor Architecture of Human Anterior Cingulate Cortex

Nicola Palomero-Gallagher[1,2], **Hartmut Mohlberg**[1], **Karl Zilles**[1,3,4], and **Brent A. Vogt**[2,5]

1 *Institute of Neurosciences and Biophysics – Medicine, Research Centre Jülich, 52425 Jülich, Germany*

2 *Cingulum Neurosciences Institute, 4435 Stephanie Drive, Manlius, NY 13104, USA*

3 *C. & O. Vogt Institute of Brain Research, Heinrich-Heine-University, 40225 Düsseldorf, Germany*

4 *Brain Imaging Centre West, Research Centre Jülich, 52425 Jülich, Germany*

5 *SUNY Upstate Medical University, 750 E. Adams Street, Syracuse, NY 13210, USA*

Abstract

Anterior cingulate cortex (ACC) is involved in emotion, emotional expression, mood and autonomic regulation in contrast to midcingulate cortex, which regulates response selection via cognitive and skeletomotor mechanisms. Although a subgenual part of ACC (sACC) may be vulnerable in depression and area 25 is cytologically unique, there are no assessments that contrast this region to pregenual ACC (pACC); both include parts of areas 32, 24, and 33 and the cingulate sulcus extends rostral to the corpus callosum and might contain area 24c. Independent verifications of cytoarchitectural differences among subregions, areas and laminar binding was undertaken with an observer-interactive approach and multireceptor autoradiography. Areas 24a and 24b have pregenual (p24a, p24b) and subgenual (s24a, s24b) components and subgenual areas have a very thin layer III. Area 24c is rostral to the genu (p24c) and has dorsal (pd24c) and ventral (pv24c) parts. Area pd24c has more and larger neurofilament-expressing neurons in layer Va and neurons in Vb form aggregates in area pv24c rather than solitary pyramids as in pd24c. Area pd24c occupies both banks of the cingulate sulcus with pv24c on the ventral bank. Layer III distinguishes these areas with pd24cd having many larger neurofilament-expressing neurons and a richer dendritic plexus in the entire layer III. Area 32 has pregenual (p32) and subgenual (s32) components. Layer II in s32 is of particular note because it has a neuron dense IIa and sparse IIb. Area 25 is comprised of anterior (25a) and posterior (25p) parts; 25p has the thinnest layer III in the cingulate gyrus and larger and more dense neurons in layer II. Area 33 continues around the genu and ventrally to encompass the full caudal extent of area 25. The multivariate, observer-interactive method accurately identified all borders except those of area 25. Finally, sACC has significantly higher $GABA_A$, $GABA_B$, BZ, α_1, and 5-HT_{1A} densities than pACC. The $GABA_B$, BZ and α_1 binding in the cingulate sulcus confirms the subdivision of area pd24c into ventral and dorsal components. Receptor binding also supports subdivision of area 25 with 25a containing significantly higher AMPA, kainate, NMDA, $GABA_A$,

Corresponding author: Nicola Palomero-Gallagher, Institute of Neurosciences and Biophysics – Medicine, Research Centre Jülich, 52425 Jülich, Germany, Phone: +49-2461-614790, e-mail: E-mail: n.palomero-gallagher@fz-juelich.de.

$GABA_B$, and α_1 receptor densities than area 25p. In conclusion, ACC is comprised of two parts that are unique in terms of their cytoarchitecture and neurotransmitter receptor organization.

Keywords

cytoarchitecture; neurofilament proteins; autoradiography; neurotransmitter; brain mapping; cingulate motor area; cortical layers

Brodmann (1909) first defined anterior cingulate cortex (ACC) and its areas 24, 32 and 33. Area 24 extended caudally to approximately the mid-level of the corpus callosum. The ACC has become a widely used concept as human functional imaging attempted to apply this nomenclauture to a single case without histological analysis (Talairach and Tournoux, 1988). Interestingly, this ACC concept has not proven useful over the last decade as no imaging paradigm has uniformly activated the ACC and the notion has arisen that it has rostral and caudal parts. There has been no explicit attempt, however, to address the problem that this is actually due to the fact that ACC is not a valid concept as conceived by Brodmann (1909) and that caudal ACC fundamentally differs from rostral ACC. That is to say, the front and back of ACC are qualitatively different in their organization and functions and the caudal "part" is not a part of ACC at all.

The midcingulate concept was introduced to draw attention to the fact that much of the posterior "part" of ACC and even some of the posterior cingulate cortex are qualitatively different from the perigenual ACC in terms of connections and functions and the differentiation of ACC and midcingulate cortex (MCC) was proposed (Vogt, 1993). The MCC is not just a caudal ACC but rather it is qualitatively unique with fundamental differences based on cytological phenotypes and other types of findings as reviewed recently (Vogt et al., 2004). These qualitative differences include the following: 1) The cytoarchitecture of MCC is characterized by large neurons in layer Vb rather than being neuron-sparse as in other regions. Also, layer IIIc has large, neurofilament-expressing neurons that are not present in ACC where layer III is thinner and generally undifferentiated. 2) The ACC regulates autonomic function by direct projections to the brainstem including those to the nucleus of the solitary tract and dorsal motor nucleus of the vagus (Neafsey et al., 1993). This region also receives most amygdala input, although a small amount does terminate in the anterior MCC (Vogt and Pandya, 1987; Vogt and Derbyshire, 2008). Finally, efferents to the spinal cord and anterior parietal lobe afferents are associated with MCC but not ACC (Baleydier and Mauguière, 1985; Cavada and Goldman-Rakic, 1989). These differences in major afferent and efferent conncections assure that qualitative differences exist in the circuitries of ACC and MCC. 3) Activation of ACC is associated with affective experiences, pleasure, and agitation and classical conditioning responses have been reported, while only fear activates the anterior part of MCC and no emotional functions have been identified yet for posterior MCC (Bancaud and Talairach, 1992; George et al., 1993; George et al., 1995; Whalen et al., 1998; Phan et al., 2002; Vogt et al., 2003). Thus, the ACC as it surrounds the genu of the corpus callosum is primarily involved in regulating autonomic and endocrine functions and is involved in conditioned emotional learning, vocalizations associated with expressing internal states, assessments of motivational content and assigning emotional valence to internal and external stimuli (Pool and Ransohoff, 1949; Talairach et al., 1973; Phan et al., 2002; Vogt et al., 2003; Vogt, 2005). None of these functions appears to be mediated primarily by the MCC. For these many reasons, the original topography of anterior cingulate cortex has been discontinued as a neurobiological construct.

The back and forth of neuroanatomical research has generated dozens of nomenclatures for cingulate cortex. One might legitimately question whether or not any reflect objective reality in the brain. To break the aparent cycle of new observations and new nomenclatures, we

evaluate the extent to which each cytoarchitectural observation receives independent verification with multivariate models of neurotransmitter receptor binding. Receptors for classical neurotransmitters are heterogeneously distributed throughout the cerebral cortex and changes in their laminar and/or regional distribution coincide with cytoarchitecturally identified areal boundaries in parietal (Scheperjans et al., 2005a; Scheperjans et al., 2005b), visual (Zilles and Clarke, 1997), auditory (Morosan et al., 2004), somatosensory (Geyer et al., 1997) and motor (Geyer et al., 1996) cortices. Quantification of multiple receptor types from different neurotransmitter systems and multivariate statistical tests provides independent means of validating hypothesis concerning cortical organization. One of the main goals of the present work is to assess the extent to which cingulate cytoarchitectural borders are validated with receptor binding methods.

There are numerous studies of single neurotransmitter systems in cingulate cortex including those for serotonin (Varnäs et al., 2004; Cannon et al., 2007), GABA (Bielau et al., 2007), and acetylcholine (Cannon et al., 2006). Among the important findings of this work is the report of highest 5-HT_{1A} receptor and serotonin transporter binding in the “subcallosal area” (Varnäs et al., 2004). A few studies approach the cingulate cortex with a multireceptor and multisystem analysis. This has been done in the monkey (Bozkurt et al., 2005) and human (Palomero-Gallagher et al., 2007a; Palomero-Gallagher et al., 2007b) cingulate cortices. This multireceptor autoradiography and multivariate statistics on human post-mortem cortex showed that subregions and areas of cingulate cortex are associated with unique receptor architecture. Thus, polar coordinate plots of 15 neurotransmitters showed, for example, that ACC and MCC differ significantly in their neurochemical composition and this approach can be used to determine markers for particular subregions and areas.

The present study of human cingulate cortex has a number of goals. First, area 25 in the monkey is relatively uniform, with a dense inner layer V–VI, a less prominent and undifferentiated layer II–III, and no layer IV (Vogt et al., 1987). Although it has been suggested that area 25 can have a dysgranular layer IV (Chu et al., 1997), this conclusion based on monkey and human studies seems to be incorrect and needs further investigation. Also, the notion of a single area 25 as suggested by Brodmann needs consideration as do the other areas that comprise sACC; i.e., areas 33, 32, and 24.

Second, an important aspect of emotional expression in primates is facial expression. The face part of the rostral cingulate motor area, which is now considered a premotor area (Vogt and Sikes, 2008), is located in area 24c, on the ventral bank of the anterior cingulate sulcus. This region projects to the facial motor nucleus (Morecraft et al., 1996) and has been activated, together with the adjacent gyral surface, by many different emotions (Vogt et al., 2003) and this provides access of multiple emotions to facial motor output. Although area 24c occupies a dorsal position in the anterior cingulate sulcus, the human anterior cingulate sulcus extends around, and in some instances rostral and ventral to, the genu of the corpus callosum. There has never been an explicit attempt to identify area 24 in this part of the cingulate sulcus. Were area 24 to occupy an extensive pregenual position, its role in emotional expression would be more profound in humans. The extent and location of area 24c and adjacent areas need consideration in this context and in relation to receptor architecture.

Third, subgenual cortex is a storage site for negatively valenced emotions (George et al., 1995; Mayberg et al., 1999) and this cortex is vulnerable to depression (Mayberg et al., 1997; Drevets et al., 1999; Drevets, 1999; Mayberg et al., 2000). We still lack a clear understanding of the essential cytological features of subgenual cortex including those of area 24 and 32 as well as area 25. Such information will provide a firmer substrate upon which to analyze cytological changes in depression and other psychiatric diseases.

Fourth, differentiation of subgenual and pregenual parts of ACC needs independent verification with multireceptor methods as does any further differentiation of cingulate areas in this region. These independent measures of structural organization are pivotal to the long-term value of such designations to future research.

Material and Methods

Postmortem Tissues and Preparation

We evaluated a total of 18 post-mortem human brains from subjects with no known history of neurological or psychiatric diseases. 4 cases (Group A) were obtained from the Derpartment of Pathology, Wake Forest University School of Medicine The remaining 14 cases (Group B, 10 cases; Group C, 4 cases) were obtained through the body donor program of the Department of Anatomy, University of Düsseldorf, Germany and were processed for the visualization of cell bodies with a modified silver staining method (group B) or for the visualization of receptors for classical neurotransmitters (group C).

Group A—Brains (2 males, 2 females; 71.5±9.8 years of age) were bisected, a medial filet removed of cingulate and adjacent cortices and digitally photographed. The cases were post-fixed in 4% paraformaldehyde for two or three days in a refrigerator and processed through a graded series of sucrose in buffer until the hemispheres sunk in 10%, 20%, and then 30%. Coronal or horizontal blocks were then cut and digitally re-photographed. The blocks were cut in a cryostat into 6 series at a 50 μm thickness and the immunohistochemical techniques below followed.

Group B—Brains (3 males, 3 females; 63±17 years of age) were removed from the skull, fixed for 5 months in Bodian's fixative or 4% formaldehyde and scanned with a T1-weighted MR sequence before subsequent histological processing. Brain MR-images were manually segmented into sequences for the left and right hemispheres to enable visualization of the hemisphere's medial surface. Surface rendering of the image sequences was performed using the software Amira (Mercury Computer Systems). After a dehydration step in graded alcohols, brains were embedded in paraffin and serially sectioned (20 om thick) in the coronal (4 cases) or horizontal (2 cases) with a large-scale microtome (20om thick serial whole-brain sections). Each 60^{th} section was mounted on gelatin-coated slides and stained for cell bodies with a silver cell body staining.

Group C—Brains (3 males, 1 female; 63±15 years of age) were bisected at autopsy and digitally photographed. Each hemisphere was cut into slabs (2–3cm thick), frozen in isopentane at −40°C and stored at −80°C in airtight plastic bags. Serial coronal cryosections (20 om, at −20°C) comprising the whole cross-section of a hemisphere were prepared using a large-scale cryostat microtome and adjacent glass-mounted sections were processed for quantitative *in vitro* receptor autoradiography according to standard protocols (Zilles et al., 2002a;b) or for the visualization of cell bodies (Merker, 1983).

Histological procedures

Silver cell body staining—Sections were stained for cell bodies with a modified silver method (Merker, 1983) which resembles Nissl staining but provides a higher contrast between cell bodies and neuropil. After removing the paraffin, sections were pretreated 4 hours with 4% formic acid diluted in distilled water followed by an overnight pre-treatment in a 10% formic acid/30% peroxide diluted in distilled water. After a thorough wash under running water and a rinse in distilled water, sections were immersed twice for 5 min. in 1% acetic acid. Sections were then placed in a physical developer under constant movement for approximately 10 min. until they become grayish. The developing step was then continued with constant

monitoring under the microscope until cell bodies were dark grey/black. The developer must be prepared immediately before use by mixing three stock solutions (Table 1) in a specific order: first 30 ml of stock solution B and then 70 ml of stock solution C are slowly added to 100 ml of stock solution A under vigorous stirring. Development was terminated by a wash in 1% acetic acid for two 5 min. periods and subsequently fixed 5 min. in a T-Max fixative (Kodak, 2 parts of T-Max and 7 parts of distilled water). Sections were dehydrated in ascending grades of alcohol (70%, 96%, 100%) for 5 min. in each dilution followed by two 5 min. immersions in xylene before coverslipping with DePex mounting medium.

Immunohistochemistry—Floating sections were pretreated with 75% methanol/25% peroxidase, followed by a 3 min pretreatment with formic acid (NeuN only) and then a washing with distilled water and two washes in phosphate buffered saline (PBS). Sections were incubated in primary antibody in PBS (dilutions: SMI32, 1:10,000, mouse; NeuN- Chemicon, Temecula, CA, 1:1,000, mouse) containing 0.3% Triton X-100 and 0.5 mg/ml bovine serum albumin (BSA) overnight at 4°C. The SMI32 antibody (Sternberger Monoclonals, Luthersville, MD) is to nonphosphorylated epitopes on the middle and heavy subunits of the neurofilament triplet. Sections were rinsed in PBS and incubated in biotinylated secondary antibody at 1:200 in PBS/Triton-X/BSA for one hour. Following rinses in PBS, sections were incubated in ABC solution (1:4; Vector) in PBS/Triton-X/BSA for one hour followed by PBS rinses and incubation in 0.05% diaminobenzidine, 0.01% H_2O_2 in a 1:10 dilution of PBS for 5 min.

After final rinses in PBS, sections were mounted, air dried, counterstained with thionin, dehydrated and cover slipped. The reaction specificity was evaluated by excluding the primary antibody from the reaction. Most sections were counterstained for 3 min in thionin (0.05%, 3.7% sodium acetate, 3.5% glacial acetic acid, pH 4.5) to ensure that all neurons are NeuN positive.

Receptor autoradiography—Fifteen different receptors of all classical neurotransmitters glutamate (AMPA, kainate, NMDA), GABA ($GABA_A$, $GABA_B$, $GABA_A$ associated benzodiazepine [BZ] binding sites), acetylcholine (M_1, M_2, M_3, nicotinic [N]), noradrenaline (a_1, a_1), serotonin (5-HT_{1A}, 5-HT_2) and dopamine (D_1) were visualized by incubating cryosections in solutions of respective tritiated receptor ligands (Table 2) according to previously published protocols (Zilles et al., 2002a;b). Binding assays involve three steps: a preincubation for removal of endogenous ligand from the tissue, the main incubation for labelling with tritiated ligands (total binding) or co-incubation of the tritiated ligand with an appropriate non-labelled displacer (nonspecific binding), and the washing step for elimination of unbound radioactive ligand from the sections.

Radioactively labelled sections were co-exposed with plastic standards of known radioactivity concentrations against tritium-sensitive films (Hyperfilm) for 4–18 weeks. The ensuing autoradiographs were processed densitometrically (Zilles et al., 2002b) after being digitized with a ProgRes C14 camera (JENOPTIK, Germany) and the KS400 image analysing software (Zeiss, Germany). The plastic standards were used to compute a transformation curve indicating the relationship between grey values in the autoradiograph and concentrations of radioactivity in the tissue.

Analytical methods

Cytological analyses—The analytical approach involved taking low magnification digital photographs (X10–40) for each antibody preparation and case with the MacroFire camera (MicroBrightField, Williston, VT). These were used to identify areas and layers of interest for higher magnification photography (X100–200). The same magnification was used for all immunoreactions in adjacent sections and the digital photographs were imported into different

layers in Photoshop CS2 and co-registered using identifiable blood vessels and surface features where available. This assured that the locations of silver stained, NeuN and SMI32-immunoreative (ir) neurons and dendritic plexi were accurately identified in each layer.

Analysis of receptor densities—Cortical areas were anatomically identified in neighbouring cell-body stained sections. Regions of interest covering the total width of the cortex and a length about twice the actual cortical depth were defined for each area, at its approximate spatial centre, as well as in the adjacent rostral and caudal sections. Thus, for each brain, area, and receptor type, three regions of interest were defined, measured and averaged to yield the absolute mean binding site densities in that particular area in fmol/mg protein. Since mean densities differed considerably between the different receptor types, they were normalized by dividing each areal density by the average receptor density of that receptor across all areas investigated before carrying out statistical tests. Receptors were evaluated for heterogeneous distribution by means of an ANOVA with repeated measures ($p<0.01$) followed by paired t-tests ($p<0.01$) to determine which area contributed to the significance.

Multivariate statistical analysis of cell density profiles—The silver stained sections from coronally sectioned brains were examined under the microscope and the centroid of each area was determined by visual inspection. Areal borders were evaluated with an algorithm-based quantification of the cortical laminar pattern (Schleicher et al., 2000; Zilles et al., 2002b; Schleicher et al., 2005). Briefly, this procedure involves four main steps: i) digitising regions of interest (ROI) in a meander-like sequence with a microscope with a motor stage for automated scanning and focusing, a CCD-camera (XC-75, Sony, Japan) and the KS400 image analysing software (Zeiss, Germany); ii) conversion of scanned ROIs into grey level index (GLI) images (Schleicher and Zilles, 1990), so that each pixel in the ensuing GLI image represents the local volume fraction of cell bodies in the corresponding measuring field; iii) extraction of equidistant profiles (3 or 6 pixels between traverses) oriented vertically to the cortical surface and layers by means of a minimum length algorithm from the GLI images, where profiles quantify the laminar GLI changes from the border between layers I and II to the border between layer VI and the white mater. iv) Multivariate statistical analysis of differences in profile shape based on the sliding window technique and computation of the Mahalanobis distance (Mahalanobis et al., 1949) as a measure of (dis)similaritiy between adjacent groups of profiles ranging from 8 to 24 profiles per block.

Results

Subregional overview

Evaluation of the ACC cytoarchitecture of each area leads to the conclusion, that cytoarchitectural features distinguish between subgenual and pregenual subregions. As a rule, the subgenual areas have a broader layer II, a relatively thin layer III, and poor differentiation of layers V and VI. Another principle of organization is that the neurons in sACC are generally much smaller and have neurofilament protein-expressing basal and apical dendrites that are short and contribute to higher neuron-packing densities. Moreover, the receptor architecture also enabled subdivision of ACC with some receptors showing higher mean (averaged over all cortical layers) subgenual densities (e.g., 5-HT_{1A}), whereas others showed the opposite (e.g., $GABA_B$).

The subgenual ACC is characterized by the confluence of several small areas and sulcal variability. These factors combined with differing planes of sectioning contribute to making this a difficult location to study. An overview of ACC subregions and areas is shown in a flat map format in Figure 1. This case has the surface features of a double parallel system of sulci (Ono et al., 1990) formed by the cingulate (cgs) and paracingulate (pcgs) sulci. Although the

pcgs forms the outer limit of cingulate cortex, the adjacent gyrus is not the “para”cingulate gyrus because it is part of cingulate cortex. Thus, the gyrus between the pcgs and cgs is referred to as the superior cingulate gyrus (SCG) even though it bends rostral to parts of the cingulate gyrus (CG) itself.

The subregions and areas are outlined in Figure 1. Area 33 is located mainly within the callosal sulcus and forms a belt around ACC. It has a pregenual component and continues as a subgenual component caudal to area 25. Area 25, which can be subdivided into an anterior (25a) and a posterior (25p) parts, is the only solely subgenual area, where it lies ventral and rostral to area 33 and caudal to areas 24 and 32. The pregenual areas 24a and 24b lie dorsal to the genu of the corpus callosum and continue ventrally to abut their counterparts in sACC. Area 24c is located on the dorsal bank of the CG and the ventral bank of the SCG and it extends rostral to the genu but not into sACC. Thus, area 24c is the only solely pregenual area of ACC. Area 32 is located mainly on the SCG, it begins in pACC dorsal to area 24 and continues rostral and ventral to the genu, and extends caudally into sACC to abut area 25.

Cytoarchitecture

Area 25—Area 25 is the area that most investigators associate with sACC, although it is not the only area in this subregion. It has a simple laminar cytoarchitecture in which layers II–III are broad, poorly differentiated, and contain evenly distributed medium-sized pyramids as shown in Figures 2 and 3. Layer V is present and contains relatively large and densely packed neurons that merge with layer VI. The cytoarchitecture of area 25 varies along its rostrocaudal extent to form two divisions: 25a and 25p.

Area 25p has a dense and broad layer II in comparison to other cingulate areas. Layer III is the thinnest of all cingulate areas, has small pyramids and is somewhat sparse in its inner part where one would expect to see a deep layer IIIc. This is also reflected in the SMI32 preparation, in which superficial layer III pyramids express neurofilament proteins while those in the deeper part do not. Layers V and VI are not distinguishable in the silver-cell-body sections or in NeuN. However, SMI32 immunoreactivity (ir) does show a particular density in layer Va.

Area 25a has a narrower and less prominent layer II than 25p, as is more characteristic of most cingulate areas. Layer III remains undifferentiated, but becomes wider and presents larger pyramids in its superficial part, as seen in all three histological preparations. This undifferentiated layer III is a general characteristic of subgenual cingulate areas, as will be described below for the subgenual components of areas 24 and 32. Layers V and VI can be distinguished, since layer V cells are larger than layer VI and in area 25p.

Area 33—Area 33 is in the depths of the callosal sulcus and has been referred to as ectogenual cortex (Braak, 1979). However, it does not end below the genu, but continues along the full caudal extent of area 25 (Fig. 2). The cytoarchitecture of area 33 is the least differentiated of any cingulate area. Layers II–III are broad and undifferentiated, while layer V has a few large pyramids occasionally standing out, and layer VI is almost non-existent.

Area 24—The most prominent features of area 24 are the lack of granular layer IV, the presence of a cell-dense layer Va and a neuron-sparse layer Vb. There are three divisions of area 24 based on progressively increasing laminar differentiation: 24a, 24b, and 24c. Area 24a abuts area 33 in the callosal sulcus, area 24b is between areas 24a and 24c, and area 24c bounds much of area 32.

Area 24a has differentiated layers II and III and a relatively thin layer Va as shown in Figures 4 and 5. Differences between the subgenual and pregenual components of area 24a are as follows:

- Layer II of area s24a is thin and these neurons form large aggregates such as the islands of neurons in entorhinal cortex. Layer II of area p24a is broader, more cell-dense and the neurons do not form aggregates.
- Layer III of area s24a contains pyramids which are larger near the surface than at the border with layer V. Layer III of p24a is wider and contains evenly distributed medium-sized pyramids which taper down in size when approaching layer V. Interestingly, the border between layers II–III is not visible in the silver-stained or NeuN sections, but can be visualized by SMI32-ir.
- Layer V is quite thin in area s24a. The layer Va pyramids of s24a are small and densely packed and the SMI32-ir dendrites are tightly packed around these neurons rather than forming large and vertically oriented clusters. This suggests that both the lateral extent of basal dendrites and vertical extent of apical dendrites are quite limited.
- Layer VI is thinner and more cell sparse in area s24a.

Area 24b has a more dense layer II, a broader and more cell-dense layer Va (the broadest layer Va in the cingulate cortex) with small pyramidal neurons intermingling with the large ones, and a more neuron-dense layer VI than area 24a (Figs. 4–5). Differences between the subgenual and pregenual components of area 24b are as follows:

- Layer II is thinner but more prominent in area s24b. In area p24b these neurons merge almost indistinguishably into layer IIIab.
- Layer III of area s24b contains large pyramids superficially and a narrow band of small neurons at the border with layer V; some of which are SMI32-ir. Layer III of area p24b contains medium-sized and uniform pyramids that taper to smaller sizes in its deeper part; layer IIIc.
- Layer Va is more densely packed in s24b as visualized with all three histolocgical preparations. Layer Vb of p24b contains more neurons than that of s24b, most of which are labelled with SMI32. In area s24b, layer Va is much broader than layer Vb, while both sublayers are approximately the same width in area p24b.
- Layer VI of area s24b is more cell dense that p24b and this layer contains many SMI32-ir neurons in both areas.

Area p24c has a broader layer II than area p24b as shown in Figures 6, 7, and 8. Layer III contains medium-sized and uniform pyramids that become less densely packed in its deeper part. Layer Va of area 24c is thinner than in p24b. It is more prominent, however, since it contains more small pyramids. Layer Vb contains many neurons; most of which are labelled with SMI32, and layer VI contains many medium-sized and SMI32-ir pyramids.

Area p24c can be subdivided into dorsal (pd24c) and ventral (pv24c) components and differences between them are as follows:

- Layer II is broader and the neurons more dispersed in area pv24c (Figs. 6–8).
- Layer III of area pd24c contains somewhat larger and SMI-ir pyramids superficially and smaller neurons at the border with layer V than is the case for area pv24c (Fig. 7).
- Layer Va is more prominent in pd24c, as clearly visualized by the SMI32-ir (Fig. 7). Layer Vb of pd24c is more densely packed than that of pv24c and neurons in pv24c tend to form small aggregates, as marked by an arrow in the magnified plate in Figure 7.

- Layer VI of area pd24c has more neurons that are slightly larger than those of area pv24c.

Area pd24c occupies both banks of the cingulate sulcus, whereas area pv24c is mainly on the ventral bank and only extends along the dorsal bank for a few millimeters where it abuts area p32. The dorsal dichotomy and ventral placement on both sides of the cgs is shown in Figure 8. Further ventral still area pv24c continues only on the ventral bank. Areas on the ventral bank of the human cingulate sulcus generally have a counterpart on the superior bank and this is true for area pd24c as well, where pd24cv is on the ventral bank and pd24cd is on the dorsal bank. Overall, the dorsal division has a generally higher level of neuron density in layers V and VI and a higher neuron and dendritic plexus expression of NFP in layers II–III. The detailed differences between these areas are as following:

- Layer II is more dispersed in area pd24cd and it has many SMI32-ir neurons which is not true for pd24cv or other cingulate areas (Fig. 6, SMI32). The presence of significant NFP expression in layer II is unique for area pd24cd.
- Layer III of area pd24cd contains large SMI32-ir pyramids which are not restricted to layer IIIc, but can also be found in layers IIIa–b (Fig. 6). Additionally, layer III of pd24cd has a much denser SMI32-ir plexus and more small pyramids (cell body staining; Figs. 6, 8) that are not SMI32-ir than does area pd24cv.
- Layer V of area pd24cd is more prominent due to the many more small and SMI32-negative neurons than in pd24cv.
- Layer VI of area pd24cd is more cell dense but pd24cv contains more SMI32-ir neurons. This means that area pd24cv has a proportionately greater density of NFP-expressing neurons in this layer than does its counterpart on the dorsal bank.

Area 32—Area 32 is a dysgranular area between agranular area 24 and granular frontal areas 9, 10 and 12. At low magnifications, area 32 is prominent for its differentiation of layers Va, Vb, and VI that appear as a pair of thin and separated layers, while its dysgranular structure is apparent only at higher magnifications in cell stains as shown in Figures 4 and 5. The presence of layer IV is also seen as a clearing or negative image in the SMI32 preparations between layers IIIc and Va. Area 32 has a broad layer II and a differentiated layer III, with large pyramids in different parts of layer III depending on the dorsoventral position. These large pyramids can form a layer IIIc dorsally or layer IIIab ventrally. These large pyramids in layer III constitute a key difference between areas 32 and 24. Another critical difference between these areas is the presence of a layer IV which is thin and, at times, contains some large layer IIIc or Va pyramids as is characteristic of a dysgranular layer.

Since cortical layer II is generally viewed to be uniform, it is particularly noteworthy that this layer has two parts in area s32. This is also the case in area 25a, though the differences between both parts are more subtle. Figure 4 shows area s32 and includes a 1.5X magnification of layer II in NeuN and SMI32 preparations. The rationale for this observation, in fact, depends on both preparations. The two pullouts in Figure 4 show the full extent of layer II which is free of SMI32-ir and the top of SMI32-ir layer III is noted with a double arrow. Reference to an adjacent and coregistered NeuN section shows that small and glabose pyramids are densely packed in superficial layer IIa. The basal dendrites on these neurons appear to be poorly formed. In contrast, Pyramids in layer IIb are less densely packed, more lancet shaped, and have a somewhat more developped basal dendritic skirt.

Differences between the subgenual (s32) and pregenual (p32) components of area 32 are as follows:

- Layer II in area s32 is discussed above. Layer II of p32 contains a few SMI32-ir neurons.
- Layer III of area p32 contains larger and more densely packed SMI32-ir pyramids; however, layer III of s32 has heavier dendritic SMI32-ir. Also, the deep layer III pyramids of area p32 are larger and more often SMI-ir when compared to those in s32.
- Layer IV is dysgranular and similar in both areas.
- Layer Va of area s32 contains slightly larger neurons and layer Vb has substantially more SMI32-ir neurons
- Layer VI contains substantially more SMI32-ir neurons in s32 than than in p32.

Multivariate statistical analysis of cell density profiles

Quantitative methods are being devised to enhance the reliability and speed of area localization in larger numbers of human brains. This will provide probability maps of the cerebral cortex including cingulate areas. To move toward this goal, we evaluated some parameters that the algorithm-based analysis uses to distinguish borders between anterior cingulate areas. An example of this evaluation with an algorithm-based quantification of the cortical laminar pattern is described for the parcellation of subgenual areas 25, 24, 32, and 33 and is shown in Figure 9.

Figures 9A and 9D show regions of interest at two rostrocaudal coronal levels from silver cell-body stained sections. In Figure 9A the section encompasses areas s33, s24a, s24b, and s32. The centroid of each area and its borders with adjacent areas were determined by visual inspection and each border marked. Figures 9B and 9C show the position of each traverse that the computer identifies as a border (number in each circle refers to the traverse at that border) when spacing between traverses was set to either 6 or 3 pixels, respectively. The visually assessed s33/s24a, s24a/s24b and s24b/s32 borders coincided in location with profiles 28, 101, and 191 (Fig. 9B), respectively. However, a spacing of only 3 pixels between traverses (Fig. 9C) led to several false-positive borders; i.e., identification of a border where one did not appear to exist, that are coded in white in Figure 9C. The black circles in Figure 9C represent correctly identified borders in A and B.

Figure 9D shows the second region of interest in a silver cell-body stained, coronal section encompassing areas s33, 25a, 25p, s24a, s24b, and s32. As described above, the centroid of each area and its borders with adjacent areas were determined and marked. Figure 9E shows the position of each traverse that the computer identifies as a border when spacing between traverses was set to 6 pixels. The visually assessed 25p/s24a, s24a/s24b and s24b/s32 borders coincided with profiles 41, 75, and 121, respectively. However, the spatial resolution provided by a 6 pixel-spacing was not sufficient to detect the s33/25a or 25a/25p borders. Therefore, we repeated the analysis with a 3 pixel spacing between traverses (Fig. 9F). With these parameters, the s33/25a and 25a/25p borders are detected at positions 37 and 64, respectively. Furthermore, the position of profiles 90, 168 and 263 (marked by black circles in Fig. 9F) coincides with that of profiles 41, 75 and 121 in Figure 9D, confirming the position of the visually detected borders between areas s24a, s24b, and s32. Additionally, the 3 pixel-spacing led to two false-positive borders within areas 24 and 32.

The same analysis was done in coronal sections for pregenual cingulate areas. The effect of 3 and 6 pixel spacing between traverses on the detection of borders between areas 33/p24a, p24a/p24b, p24b/pd24cv, pd24cv/pd24cd, and pd24cd/p32 were evaluated. Again, the 3 pixel spacing led to varying numbers of false-positives, whereas the borders detected with the 6 pixel spacing coincided in location with the visually assessed 33/p24a, p24a/p24b, p24b/pd24cv,

pd24cv/pd24cd, and pd24cd/p32 borders. Thus, a traverse spacing of 3 pixels led to an overparcellation of pACC, while the 6 pixel spacing most acurately identified each border in this subregion.

The quantitative assesment of cytological borders using the algorithm-based quantification of the laminar pattern is sensitive to factors such as the distence between traverses as well as the unique features of each area being analized. This analysis showed that spacing between profiles could generally be set to 6 pixels. However, for subdivisions of area 25, spacing between profiles had to be reduced to 3 pixels in order to provide sufficient spatial resolution.

Receptor Architecture

Receptor architecture studies sought to provide independent markers of neuronal phenotype to validate distinctions based on neuron architecture by identifying the unique neurotransmitter features that might verify the subgenual/pregenual dichotomy of ACC. Receptors for classical neurotransmitters present distinct laminar distribution patterns throughout pACC as shown in Figures 10 and 11. Some receptors have higher densities in superficial layers with maxima in either layers I–II (5-HT_{1A}) or II–III and IV when present (AMPA, NMDA, $GABA_A$, $GABA_B$, BZ, M_1, M_3, a_1, a_2 and D_1). Other receptors have the opposite pattern, with highest binding in the deep layers (kainate, M_2). The 5-HT_2 receptors present a single local maximum in layer III. Nicotinic receptors present two local maxima in layers I and III.

Neurotransmitter binding presents distinct laminar patterns throughout sACC (Figs. 10 and 11). Some receptors present the same distribution in sACC areas 24 and 32 as in their pACC counterparts (kainate, M_2, α_1, α_2, 5-HT_{1A}, 5-HT_2, D_1), whereas other receptors differ: AMPA, NMDA, $GABA_A$, $GABA_B$, BZ and M_3 binding has homogeneously distributed over all layers; nicotinic receptors present a single maximum in layer I. Area 25 is caudal to area 25 (Figs. 10 and 11) and AMPA, M_3, and 5-HT_{1A} receptor densities are higher in its superficial layers. Kainate and M_2, receptors show the opposite distribution, with higher densities in the deep layers. NMDA, $GABA_A$, $GABA_B$, BZ, nicotinic, α_1, α_2, and 5-HT_2 receptors are homogeneously distributed throughout area 25

To address the question as to which neurotransmitter receptors differentiate the subgenual and pregenual components of ACC, we calculated the receptor polar coordinate plot (fingerprint) of each subregion by averaging the mean densities (over all layers) of all areas present in that subregion as shown in Figure 12a. Thus, the fingerprint for sACC contains the mean densities of areas 25a, 25p, 33, s24a, s24b, and s32. Similarly, the fingerprint of pACC comprises the mean densities of areas 33, p24a, p24b, p32 and all subdivisions of area p24c. Statistical analysis revealed that sACC contains significantly higher $GABA_A$, $GABA_B$, BZ, α_1, and 5-HT_{1A} densities than pACC. Although M_3 and 5-HT_2 receptor densities tended to be higher in sACC (Fig. 11), they did not reach significance.

Distributions of receptors for GABA, norepinephrin and dopamine provide further evidence concerning the subdivision of area pd24c into its ventral and dorsal counterparts (Figs. 10 and 11). Statistical analysis of receptor densities in the superficial and deep layers of areas pd24cv and pd24cd revealed following significant differences at $p<0.01$: $GABA_B$, BZ, and D_1 densities were significantly higher in layers I–III of area pd24cv (Fig. 13a). Additionally α_1 receptor densities were higher in all layers of pd24cv (Fig. 13).

Receptor binding supports the subdivision of area 25 into anterior and posterior components. The laminar distributions of binding is comparable in areas 25a and 25p; however, both areas differ considerably in their receptor fingerprints (Fig. 12b). Area 25a contains significantly higher ($p<0.01$) AMPA, kainate, NMDA, $GABA_A$, $GABA_B$, and α_1 receptor densities than area 25p.

Discussion

The present findings flow from a multimodal data analysis. They involve the integration of observations from silver cell-body stains, immunocytochemistry and receptor autoradiography. The combination of these varied methods enables both an independent verification of cytological with receptor architecture and provides for devising integraterd models of circuit organization. In the former instance, for example, it was found that receptor fingerprints for sACC significantly differed from those of pACC, thus confirming histological distinctions. In the latter instance, modulation of the the amygdalocingulate circuitry is proposed below based on a combination of glutamate and 5-HT_{1A} receptor colocalization in particular layers of sACC.

Dichotomy of ACC

Studies of emotion and mood disorders have emphasized subgenual cortex as possibly having a selective vulnerability in major depression (Mayberg et al., 1997; Drevets et al., 1999; Mayberg et al., 2000; Phan et al., 2002; Vogt, 2005). Although the depression literature proposes many cell-level mechanisms, which can't be reviewed here, there has been no cytoarchitectural study comparing how laminar histology in this region is disordered by this disease(s). One of the goals of this research has been to provide a normative basis for such work and to verify its veracity with polar coordinate plots of receptor densities.

Although area 25 is the largest component of sACC and it dominates our thinking about this subregion, its border with pACC is determined by areas 32 and 24. We define the border between these subregions based on a thick layer II and a very thin layer III in both areas 24 and 32. Thus, subgenual area 32 has a striking layer II that is differentiated into two parts, and a very thin layer III. Based on these criteria, there are subgenual extensions of both areas 24 and 32.

The first two studies of 15 transmitter receptors in cingulate cortex provided independent verification of the four regions and most subregions in cingulate cortex as an extention of neurocytological observations (Palomero-Gallagher et al., 2007b; Palomero-Gallagher and Zilles, 2008). Indeed, the former (2007) of these two reports establishes the expectation for the ACC dichotomy that has been systematically considered here. These receptor studies focus attention on the unique features of transmitter systems in each subregion, since the receptor fingerprints of pregenual and subgenual cortices clearly show that these regions differ. Some neurotransmitter systems are responsible for differentiating the functions of these regions, and we found significant density differences between sACC and pACC for the serotoninergic and GABAergic systems. The 5-HT_{1A} receptor density was significantly higher in sACC than in pACC. This finding is in accordance with the higher 5-HT_{1A} receptor densities measured by Varnäs et al. (2004) in the "subcallosal area" than in the anterior cingulate gyrus. Further consideration of the functional significance of this system is discussed below in the context of circuit functions.

The $GABA_A$, $GABA_B$ and BZ binding densities were higher in sACC than in pACC. Sad memories are stored in sACC. One wonders whether the high level of GABAergic activity in sACC isolates the memories of these sad events from and stops them from "over-participting" in conscious processes, since one would assume that constant access to sad memories would produce an altered mood. This hypothesis is bolstered by the observations that recurrent depression could be associated with decreased GABA levels in ACC (Bhagwagar et al., 2007).

Layer II dichotomy and circuitry in sACC

A characteristic of periallocortical areas is the presence of "extraverted" pyramidal neurons (Sanides and Sanides, 1972). Cajal (Ramón y Cajal, 1922) described large star cells in layer II of entorhinal cortex that had extensive dendritic ramifications throughout layer I. Similarly, large or extraverted pyramids have been reported in retrosplenial area 29 (Vogt and Peters, 1981). The neurons in layer IIa of areas s32 and 25a tend to be globular rather than lancet-shaped, like neurons of layer IIb, and likely fit the "extraverted" pyramidal criteria with weak basal dendrite elaboration.

One would predict that intralaminar specializations in structure are associated with unique features of circuit function. Since the primary termination site of the amygdala in ACC is layer II (Amaral and Price, 1984; Vogt and Pandya, 1987), it is likely that the amygdala largely governs the output of layer II. Although we don't know the exact postsynaptic targets, this input is in deep layer I as well as in layer II and could have a prefferential impact on layer IIa function. A relay from layer II to deeper layers has been proposed in neocortex (Thompson et al., 2002) and may also be the case for this region. Layer III of ACC provides the primary outflow to other cortical areas including dorsolateral prefrontal, orbitofrontal, rostral superior temporal sulcal cortex and ventral posterior cingulate cortex (Vogt and Pandya, 1987). To the extent that layer III is very thin in sACC, these cortical projections must be relatively weak in comparisson to corticocortical connections of other regions including pACC. Moreover, the relative importance of amygdalar afferents in sACC and the layer II projection to layer III is likely to be much greater than is the case for pACC where layer III is more expanded and the relative significance of amygdalar input is reduced.

Since AMPA and NMDA receptors are located preferentially in superficial layers of sACC, they might mediate amygdalar input to these areas, which is thought to be a glutamatergic projection (Zhuo, 2007). Furthermore, the presence of high 5-HT_{1A} receptors in layers I–II suggests that serotonin could amplify the amygdalar signal and further drive output from layer III neurons. Thus, the multireceptor analysis provides a starting point for understanding specific circuits in sACC.

Divisions and extent of area 24c

Area 24c is located in the most rostral extent of the cingulate sulcus in human (Vogt et al., 1995) and monkey (Vogt et al., 2005). One of the primary issues explored in this study is the extent to which area 24c follows the cingulate sulcus in the human, where it lies rostral to the genu of the corpus callosum, and not just dorsally, as is the case in monkeys. The importance of area 24c derives from its projections to the facial motor nucleus (Morecraft et al., 1996) and the importance of facial expression in the expression of emotion. This region has been activated, together with the adjacent gyral surface, by many different emotions (Vogt et al., 2003) and this provides access of multiple emotions to facial motor output. To the extent that area 24c is greatly expanded in the human brain, it is expected that a wider range of emotions might have access to facial expression.

Area 24c might be one of the cytologically most heterogeneous areas in the cingulate cortex. It is located within the cingulate sulcus and extends rostral, though not ventral, to the genu of the corpus callosum. Therefore, area 24c is a solely pregenual component of ACC and has been renamed area p24c. The cytoarchitecture of p24c varies along its dorsoventral course, thus enabling the definition of a ventral portion located directly rostral to the genu (area pv24c), and of a dorsal component (area pd24c) found dorsal to the genu and abutting aMCC. The main architectonic differences between areas pd24c and pv24c are the broader and more dispersed layer II and the clusters of neurons in layer Vb of pv24c. Also, there is a more prominent and SMI32-ir layer Va and a more densely packed layer Vb in area pd24c. To the extent that area

24c is greatly expanded in the human brain, it is expected that a wider range of emotions might have access to facial expression. The presence of a dorsal and a ventral subdivision in human area p24c might imply that these two areas are differentially involved in the facial expression of emotions. Many of these elaborations of p24c may not have direct facial motor projections.

Layer Vb is the origin for spinal and brainstem motor output (Dum and Strick, 1991) and monkey area 24c contains the face part of the rostral cingulate motor area (Morecraft et al., 1996). Interestingly, in the monkey, area p24c is on the ventral bank of the rostral cingulate sulcus; thus, monkeys do not have an area pv24c. In humans, area pv24c is mainly on the ventral bank of the cingulate sulcus, and area pd24c extends over both banks and has two divisions: area pd24cv on the ventral bank and area pd24cd on the dorsal bank. The main architectonic differences between these two areas are the presence of numerous SMI32-ir neurons in layer II of area pd24cd but not in pd24cv or other cingulate areas. Also, area pd24cv has a proportionately greater density of NFP-expressing neurons in layer VI than does area pd24cd.

The receptor architecture of area pd24c confirms histological observations of a subdivision of this area (Palomero-Gallagher et al., 2007b; Palomero-Gallagher and Zilles, 2008), and we found that receptor fingerprints for the superficial layers of pd24cv and pd24cd differed significantly from those of the deep layers. This dorsoventral dichotomy of area pd24c is continued caudally along the human cingulate sulcus, since areas on its ventral bank generally have a counterpart on the superior bank, i.e., areas 24c'v/24c'd and 24dv/24dd (Vogt and Vogt, 2003).

Periallocortical areas

Area 33 does not end below the genu of the corpus callosum as described by Brodmann (1909), but continues along the full caudal extent of area 25. Thus, area 33 forms a border around the caudal portion of ACC, as previously observed in cell body and myelin stanined histological sections (Vogt, 1910; von Economo and Koskinas, 1925; Sarkissov et al., 1955).

Area 25 in the monkey is striking in that it has essentially uniform superficial layers I–III and deep layers V–VI (Vogt et al., 1987). When searching for the centroid of area 25 in the human, therefore, we were not able to include cortex with layer IV as done by Chu et al. (1997), who identified a dsygranular area 25, and our area 25 does not have a layer IV. The difficulty assessing sACC is that it forms a confluence with areas 24 and 32. Indeed, in instances where we saw clear differentiation of layers V, including a layer Va and Vb, and VI we also found a dysgranular layer IV and identified area 32. Thus, confusion generated over various nomenclatures for area 25 can be solved by using careful criteria that exclude a layer IV.

Multivariate statistical analysis of cell density profiles

A pivotal application of cytoarchitetural information, as that described here, will eventually be made to generate probability maps from large groups of post-mortem cases. An algorithm-based, quantification method of cortical laminar patterns is available that is observer-interactive, enhances the reliability and speed of area localization in large brain samples and provides a supplement to the visual, microscopical assessment of area centroids and boundaries (Schleicher et al., 1999). It is based on the fact that each area has a distinctive laminar pattern, which can be represented by profile curves extending from the border between layers I and II to the white matter boundary and extracted from equidistant traverses defined perpendicularly to the cortical surface. The degree of (dis)similarity in the shape of groups (blocks) of neighbouring profiles, can be quantitatively expressed as a Mahalanobis distance and maxima in this function tested for statistical significance (Schleicher et al., 1999). The spatial resolution

and sensitivity of this procedure are determined, among others, by the spacing between traverses, the number of profiles per block, and the unique features of each area being analized.

In a recent study, Caspers et al. (Caspers et al., 2006) dynamically adapted their border detection-threshold to ensure sufficient sensitivity of the quantitative cytoarchitectonic analysis of the human inferior parietal cortex, while avoiding false positive parcellations. Of the seven examined areas, two had very similar cytoarchitectonic patterns and the border between them could not be detected with the standard setting of 6 pixel spacing between traverses and a range of 8–24 profiles per block for computation of distances. For this specific pair of areas, they increased sensitivity by reducing the threshold, i.e., by reducing the number of profiles per block to less than 8, for partitioning the cortical strip. In the present study we found that the standard settings were adequate to detect the majority of borders. However, the spatial resolution provided by the 6 pixel spacing was not sufficient to enable detection of the border between areas 25a and 25p, since these are two particularly small areas. Therefore, it was necessary to adapt the threshold to increase sensitivity. We did this by reducing the spacing between traverses from 6 to 3 pixels, i.e., by doubling the number of profiles that could be extracted from a single area and that could subsequently be used for the multivariate statistical analysis.

In the present study, we have used a multimodal approach to determine the cytological and receptor architectural features that characterize the subregions and areas of ACC. This approach not only enabled the independent verification of area boundaries, but also provided a rationale for differentiating the subgenual and pregenual parts of the ACC. This observer-interactive method and the criteria for each ACC area can now be applied to large samples of postmortem cases to generate probability maps for this region.

Acknowledgements

We thank Leslie Vogt, Nadine Dechering and Ursula Blohm for excellent technical assistance. This Human Brain Project/Neuroinformatics research was funded jointly by the National Institute of Mental Health, of Neurological Disorders and Stroke, of Drug Abuse, and the National Cancer Centre (KZ) and NIH-NINDS grant RO1 NS44222 (BAV).

Reference List

Amaral DG, Price JL. Amygdalo-cortical projections in the monkey (Macaca fascicularis). J Comp Neurol 1984;230:465–496. [PubMed: 6520247]

Baleydier C, Mauguière F. Anatomical evidence for medial pulvinar connections with the posterior cingulate cortex, the retrosplenial area, and the posterior parahippocampal gyrus in monkeys. J Comp Neurol 1985;232:219–228. [PubMed: 3973091]

Bancaud J, Talairach J. Clinical semiology of frontal lobe seizures. Adv Neurol 1992;57:3–58. [PubMed: 1543059]

Bhagwagar Z, Wylezinska M, Jezzard P, Evans J, Boorman E, Matthews M, Cowen J. Low GABA concentrations in occipital cortex and anterior cingulate cortex in medication-free, recovered depressed patients. Int J Neuropsychopharmacol 2007:1–6. [PubMed: 17470315][Eupub ahead of print]

Bielau H, Steiner J, Mawrin C, Trubner K, Brisch R, Meyer-Lotz G, Brodhun M, Dobrowolny H, Baumann B, Gos T, Bernstein HG, Bogerts B. Dysregulation of GABAergic neurotransmission in mood disorders: a postmortem study. Ann N Y Acad Sci 2007;1096:157–169. [PubMed: 17405927]

Bozkurt A, Zilles K, Schleicher A, Kamper L, Sanz Arigita E, Uylings HB, Kötter R. Distributions of transmitter receptors in the macaque cingulate cortex. Neuroimage 2005;25:219–229. [PubMed: 15734357]

Braak H. Pigment architecture of the human telencephalic cortex. V. Regio anterogenualis. Cell Tiss Res 1979;204:441–451.

Brodmann, K. Vergleichende Lokalisationslehre der Groβhirnrinde in ihren Prinzipien dargestellt auf Grund des Zellbaues. Leipzig: Barth; 1909.

Cannon DM, Carson RE, Nugent AC, Eckelman WC, Kiesewetter DO, Williams J, Rollis D, Drevets M, Gandhi S, Solorio G, Drevets WC. Reduced muscarinic type 2 receptor binding in subjects with bipolar disorder. Arch Gen Psychiatry 2006;63:741–747. [PubMed: 16818863]

Cannon DM, Ichise M, Rollis D, Klaver JM, Gandhi SK, Charney DS, Manji HK, Drevets WC. Elevated Serotonin Transporter Binding in Major Depressive Disorder Assessed Using Positron Emission Tomography and [(11)C]DASB; Comparison with Bipolar Disorder. Biol Psychiatry. 2007

Caspers S, Geyer S, Schleicher A, Mohlberg H, Amunts K, Zilles K. The human inferior parietal cortex: Cytoarchitectonic parcellation and interindividual variability. Neuroimage 2006;33:430–448. [PubMed: 16949304]

Cavada C, Goldman-Rakic PS. Posterior parietal cortex in rhesus monkey: I. Parcellation of areas based on distinctive limbic and sensory corticocortical connections. J Comp Neurol 1989;287:393–421. [PubMed: 2477405]

Chu C-C, Tranel D, Damasio AR, Van Hoesen GW. The autonomic-related cortex: Pathology in Alzheimer's disease. Cereb Cortex 1997;7:86–95. [PubMed: 9023436]

Drevets WC. Prefrontal Cortical-Amygdalar Metabolism in Major Depression. Ann NY Acad Sci 1999;877:614–637. [PubMed: 10415674]

Drevets WC, Frank E, Price JC, Kupfer DJ, Holt D, Greer PJ, Huang Y, Gautier C, Mathis C. PET imaging of serotonin 1A receptor binding in depression. Biol Psychiatry 1999;46:1375–1387. [PubMed: 10578452]

Dum RP, Strick PL. The origin of corticospinal projections from the premotor areas in the frontal lobe. J Neurosci 1991;11:667–689. [PubMed: 1705965]

George MS, Ketter TA, Gill DS, Haxby J, Ungerleider L, Herscovitch P, Post RM. Brain regions involved in recognizing facial emotion or identity: An oxygen-15 PET study. J Neuropsychiat Clin Neurosci 1993;5:384–394.

George MS, Ketter TA, Parekh PI, Horwitz B, Herscovitch P, Post RM. Brain activity during transient sadness and happiness in healthy women. Am J Psychiatry 1995;152:341–351. [PubMed: 7864258]

Geyer S, Ledberg A, Schleicher A, Kinomura S, Schormann T, Bürgel U, Klingberg T, Larsson J, Zilles K, Roland PE. Two different areas within the primary motor cortex of man. Nature 1996;382:805–807. [PubMed: 8752272]

Geyer S, Schleicher A, Zilles K. The somatosensory cortex of human: Cytoarchitecture and regional distributions of receptor-binding sites. Neuroimage 1997;6:27–45. [PubMed: 9245653]

Mahalanobis PC, Majumda DN, Rao CR. Antropometric survey of the united provinces. A statistical study. Sankhya 1949;9:89–324.

Mayberg HS, Brannan SK, Mahurin RK, Jerabek PA, Brickman J, Tekell JL, ET AL. Cingulate function in depression: a potential predictor of treatment response. NeuroReport 1997;8:1057–1061. [PubMed: 9141092]

Mayberg HS, Brannan SK, Tekell JL, Silva JA, Mahurin RK, McGinnis S, Jerabek PA. Regional metabolic effects of fluoxetine in major depression: serial changes and relationship to clinical response. Biol Psychiatry 2000;48:830–843. [PubMed: 11063978]

Mayberg HS, Liotti M, Brannan SK, McGinnis S, Mahurin RK, Jerabek PA, Silva JA, Tekell JL, Martin CC, Lancaster JL, Fox PT. Reciprocal limbic-cortical function and negative mood: converging PET findings in depression and normal sadness. Am J Psychiatry 1999;156:675–682. [PubMed: 10327898]

Merker B. Silver staining of cell bodies by means of physical development. J Neurosci Methods 1983;9:235–241. [PubMed: 6198563]

Morecraft RJ, Schroeder CM, Keifer J. Organisation of face representation in the cingulate cortex of the rhesus monkey. NeuroReport 1996;7:1343–1348. [PubMed: 8856672]

Morosan, P.; Rademacher, J.; Palomero-Gallagher, N.; Zilles, K. Anatomical organization of the human auditory cortex: Cytoarchitecture and transmitter receptors. In: Heil, P.; König, E.; Budinger, E., editors. Auditory Cortex – Towards a Synthesis of Human and Animal Research. New Jersey: Lawrence Erlbaum, Mahwah; 2004. p. 27-50.

Neafsey, EJ.; Terreberry, RR.; Hurley, KM.; Ruit, KG.; Frysztak, RJ. Anterior cingulate cortex in rodents: connections, visceral control functions, and implications for emotion. In: Kolb, B.; Tees, RC., editors. The Cerebral Cortex of the Rat. Cambridge, MA: MIT; 1993. p. 206-223.

Ono, M.; Kubik, S.; Abernathey, CD. Atlas of the cerebral sulci. Stuttgart, New York: Thieme Verlag; 1990.

Palomero-Gallagher N, Mohlberg H, Zilles K, Vogt BA. Receptor- and cytoarchitecture of human anterior cingulate cortex. J Comp Neurol. 2007ain preparation

Palomero-Gallagher N, Vogt BA, Mayberg HS, Schleicher A, Zilles K. Receptor architecture of human cingulate cortex: insights into the four-region neurobiological model. Cerebral Cortex. 2007bsubmitted

Palomero-Gallagher, N.; Zilles, K. Transmitter Receptor Systems in Cingulate Regions and Areas. In: Vogt, BA., editor. Cingulate Neurobiology & Disease, volume 1: Infrastructure, Diagnosis, Treatment. Oxford University Press; 2008.

Phan KL, Wager T, Taylor SF, Liberzon I. Functional neuroanatomy of emotion: a meta-analysis of emotion activation studies in PET and fMRI. Neuroimage 2002;16:331–348. [PubMed: 12030820]

Pool JL, Ransohoff J. effects on stimulating rostral portion of cingulate gyri in man. J Neurophysiol 1949;12:385–392. [PubMed: 15408005]

Ramón y Cajal S. Estudios sobre la fina estructura de la corteza regional de los roedores. I. corteza suboccipital (Retrosplenial de Brodmann). Trab Lab Biol Univ Madrid 1922;20:1–30.

Sanides F, Sanides D. The “extraverted neurons” of the mammalian cerebral cortex. Z Anat Enwicklungsgesch 1972;136:272–293.

Sarkissov, SA.; Filimonoff, IN.; Kononowa, EP.; Preobrachenskaja, IS. Atlas of the Cytoarchitectonics of the Human Cerebral Cortex. Moscow: Medgiz; 1955.

Scheperjans F, Grefkes C, Palomero-Gallagher N, Schleicher A, Zilles K. Subdivisions of human parietal area 5 revealed by quantitative receptor autoradiography: a parietal region between motor, somatosensory and cingulate cortical areas. Neuroimage 2005a;25:975–992. [PubMed: 15808998]

Scheperjans F, Palomero-Gallagher N, Grefkes C, Schleicher A, Zilles K. Transmitter receptors reveal segregation of cortical areas in the human superior parietal cortex: Relations to visual and somatosensory regions. Neuroimage 2005b;28:362–379. [PubMed: 16054841]

Schleicher A, Amunts K, Geyer S, Kowalski T, Schormann T, Palomero-Gallagher N, Zilles K. A stereological approach to human cortical architecture: identification and delineation of cortical areas. J Chem Neuroanat 2000;20:31–47. [PubMed: 11074342]

Schleicher A, Amunts K, Geyer S, Morosan P, Zilles K. Observer-independent method for microstructural parcellation of cerebral cortex: A quantitative approach to cytoarchitectonics. Neuroimage 1999;9:165–177. [PubMed: 9918738]

Schleicher A, Palomero-Gallagher N, Morosan P, Eickhoff SB, Kowalski T, de VK, Amunts K, Zilles K. Quantitative architectural analysis: a new approach to cortical mapping. Anat Embryol (Berl) 2005;210:373–386. [PubMed: 16249867]

Schleicher A, Zilles K. A quantitative approach to cytoarchitectonics: analysis of structural inhomogeneities in nervous tissue using an image analyser. J Microsc 1990;157:367–381. [PubMed: 2332886]

Talairach J, Bancaud J, Geier S, Bordas-Ferrer M, Bonis A, Szikla G. The cingulate gyrus and human behavior. Electroencephalogr Clin Neurophysiol 1973;34:45–52. [PubMed: 4118434]

Talairach, J.; Tournoux, P. Co-planar stereotaxic atlas of the human brain. Stuttgart, New York: Thieme; 1988.

Thompson AM, West DC, Wang Y, Bannister AP. Synaptic connections and small circuits involving excitatory and inhibitory neurons in layers 2–5 of adult rat and cat neocortex - triple intracellular recordings and biocytin labelling in vitro. Cerebral Cortex 2002;12:936–953. [PubMed: 12183393]

Varnäs K, Halldin C, Hall H. Autoradiographic distribution of serotonin transporters and receptor subtypes in human brain. Human Brain Mapping 2004;22:246–260. [PubMed: 15195291]

Vogt BA. Pain and emotion interactions in subregions of the cingulate gyrus. Nature Reviews Neuroscience 2005;6:533–544.

Vogt BA, Berger GR, Derbyshire SWG. Structural and functional dichotomy of human midcingulate cortex. Eur J Neurosci 2003;18:3134–3144. [PubMed: 14656310]

Vogt, BA.; Derbyshire, SWG. Visceral circuits, autonomic functions & human imaging. In: Vogt, BA., editor. Cingulate Neurobiology & Disease, volume 1: Infrastructure, Diagnosis, Treatment. Oxford University Press; 2008.

Vogt BA, Nimchinsky EA, Vogt L, Hof PR. Human cingulate cortex: surface features, flat maps, and cytoarchitecture. J Comp Neurol 1995;359:490–506. [PubMed: 7499543]

Vogt BA, Pandya DN. Cingulate cortex of the rhesus monkey: II. Cortical afferents. J Comp Neurol 1987;262:271–289. [PubMed: 3624555]

Vogt BA, Pandya DN, Rosene DL. Cingulate cortex of the rhesus monkey: I. Cytoarchitecture and thalamic afferents. J Comp Neurol 1987;262:256–270. [PubMed: 3624554]

Vogt BA, Peters A. Form and distribution of neurons in rat cingulate cortex: Area 32, 24 and 29. J Comp Neurol 1981;195:603–625. [PubMed: 7462444]

Vogt, BA.; Sikes, RW. Cingulate nociceptive circuitry and roles in pain processing: the cingulate premotor pain model. In: Vogt, BA., editor. Cingulate Neurobiology & Disease, volume 1: Infrastructure, Diagnosis, Treatment. Oxford University Press; 2008.

Vogt BA, Vogt L. Cytology of human dorsal midcingulate and supplementary motor cortices. J Chem Neuroanat 2003;26:301–309. [PubMed: 14729132]

Vogt BA, Vogt L, Farber NB, Bush G. Architecture and neurocytology of monkey cingulate gyrus. J Comp Neurol 2005;485:218–239. [PubMed: 15791645]

Vogt O. Die myeloarchitektonische Felderung des menschlichen Stirnhirns. Journal für Psychologie und Neurologie 1910;15:221–232.

von Economo, C.; Koskinas, GN. Die Cytoarchitektonik der Hirnrinde des erwachsenen. Menschen, Wien, Berlin: Springer; 1925.

Whalen PJ, Bush G, McNally RJ, Wilhelm S, McInerney SC, Jenike MA, Rauch SL. The emotional counting Stroop paradigm: a functional magnetic resonance imaging probe of the anterior cingulate affective division. Biol Psychiatry 1998;44:1219–1228. [PubMed: 9861465]

Zhuo M. A synaptic model for pain: long-term potentiation in the anterior cingulate cortex. Mol Cells 2007;23:259–271. [PubMed: 17646700]

Zilles K, Clarke S. Architecture, connectivity, and transmitter receptors of human extrastriate visual cortex. Comparison with nonhuman primates. Cerebral Cortex 1997;12:673–742.

Zilles K, Palomero-Gallagher N, Grefkes C, Scheperjans F, Boy C, Amunts K, Schleicher A. Architectonics of the human cerebral cortex and transmitter receptor fingerprints: reconciling functional neuroanatomy and neurochemistry. European Neuropsychopharmacology 2002a;12:587–599. [PubMed: 12468022]

Zilles, K.; Schleicher, A.; Palomero-Gallagher, N.; Amunts, K. Quantitative analysis of cyto- and receptorarchitecture of the human brain. In: Toga, AW.; Mazziotta, JC., editors. Brain Mapping. The Methods. Amsterdam: Elsevier; 2002b. p. 573-602.

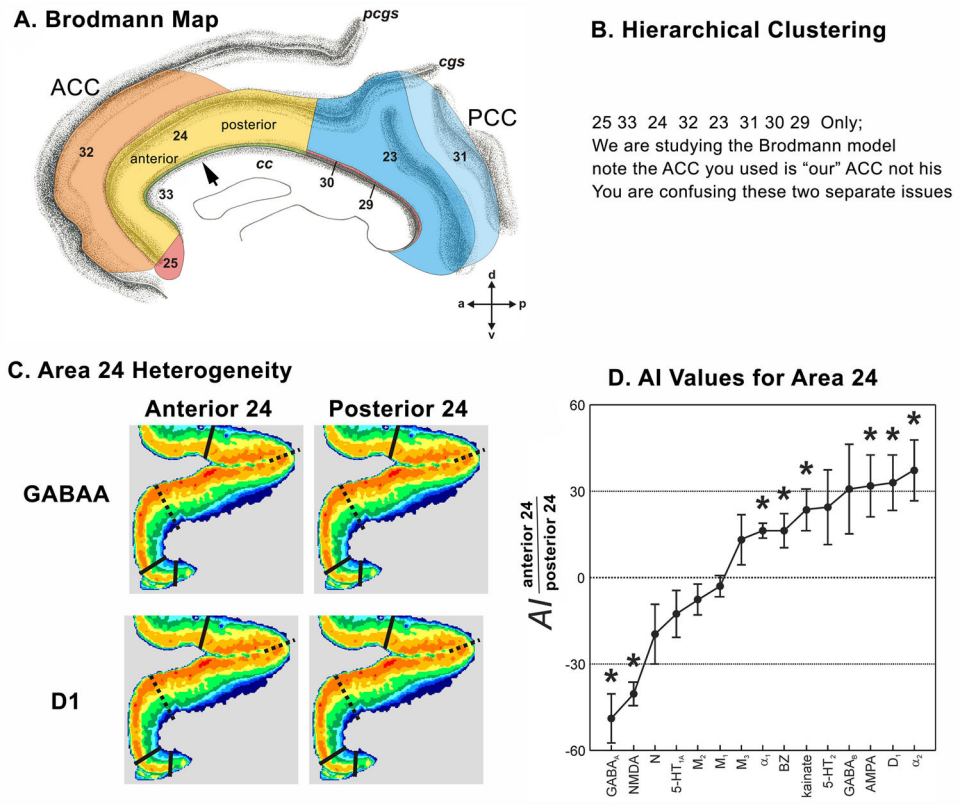

Figure 1.

Flat map of the medial surface of the human anterior cingulate cortex showing the distribution of subregions and areas from a histological assessment. The sulcal depths are noted with a homogeneous gray color. *CC*: corpus callosum; *CG*: cingulate gyrus; *SCG*: superior cingulate gyrus; *SFG*: superior frontal gyrus; *cas*: callosal sulcus; *cgs*: cingulate sulcus; *pcgs*: paracingulate sulcus.

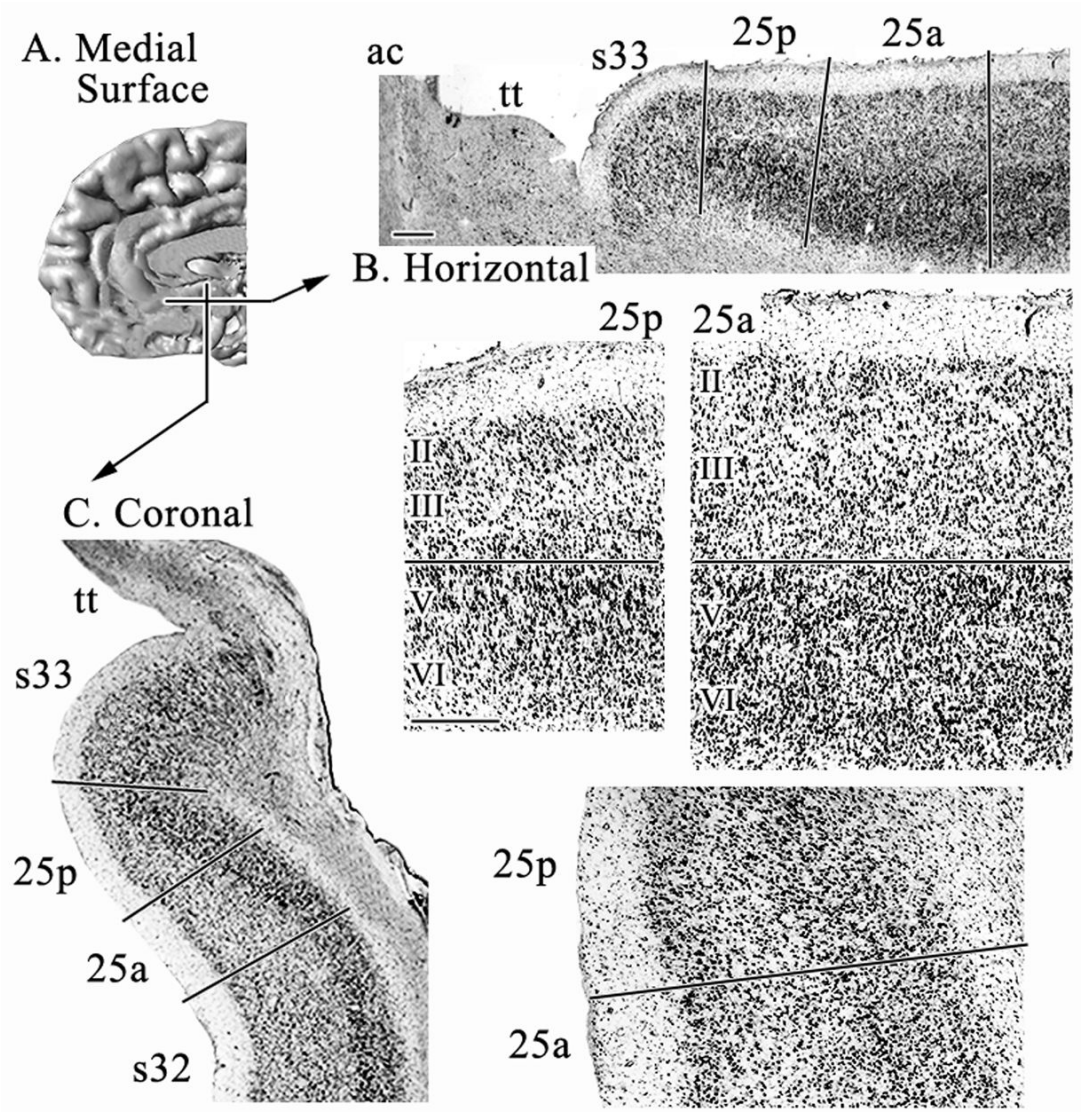

Figure 2.

A. Medial surface of a reconstructed human hemisphere visualizing the two levels from which sections shown in B and C were taken. **B.** and **C.** are low magnifications of horizontal (B) and coronal (C), cell-body stained sections in which the relative positions of subgenual areas 33, 25 and 32 are shown. Area 25a lies rostral and dorsal to area 25p. **D.** Micrographs of areas 25a and 25p magnified from B. **E.** Micrographs of areas 25a and 25p magnified from C. Layer II is more prominent and layers V and VI are not differentiated in area 25p. Layers in this and subsequent figures are aligned at the border between layer III (or IV when present) and the top of layer V. Roman numerals indicate cortical layers. *ac*: anterior commissure; *tt*: taenia tecta. Scale bars = 500 om.

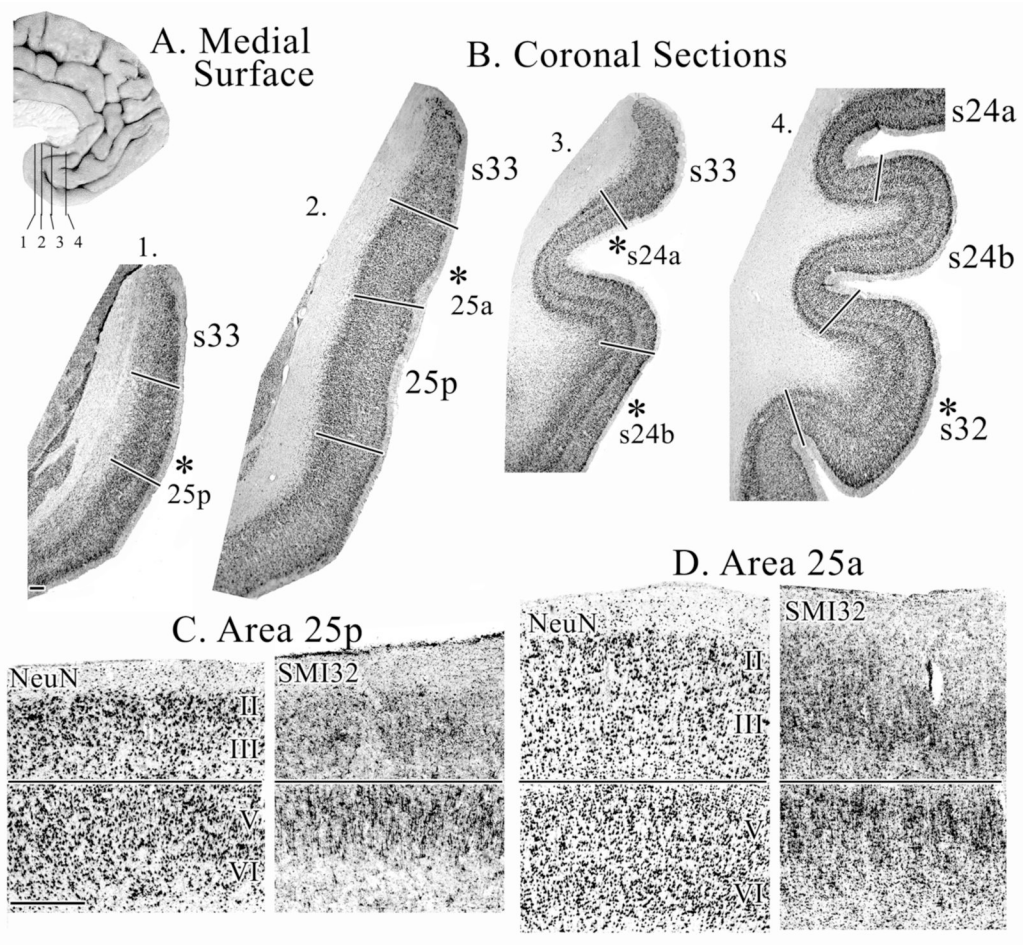

Figure 3.

A. Medial surface of a human hemisphere showing four levels used in B. **B.** Coronal sections immunoreacted with NeuN antibody through different rostrocaudal levels of sACC. Asterisks indicate the position from which micrographs shown in C, D, and Figure 4 were taken. Sections for SMI32-ir were adjacent to the NeuN sections. **C.** Micrographs of area 25p show large, densely packed layer II neurons and a very thin layer III **D.** Micrographs of area 25a showing a wider, but still undifferentiated, layer III. Scale bars = 500 om.

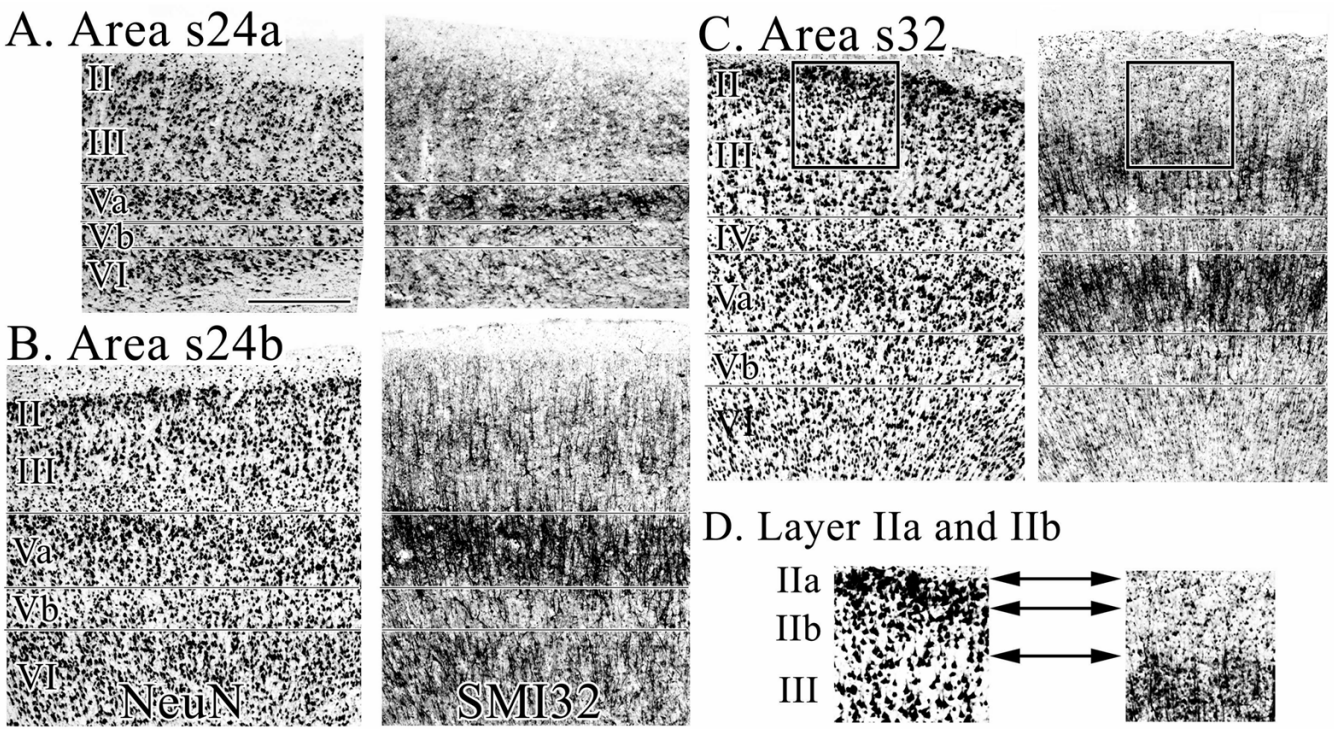

Figure 4.

Micrographs of areas s24a, s24b, and s32 immunoreacted for NeuN and SMI32 **A.** Area s24c has a thin layer II in which neurons form large aggregates and the small and densely packed layer Va pyramids have tightly packed SMI32-ir dendrites. **B.** Area s24b has a cell-dense layer Va and numerous SMI32-ir neurons in layer VI. **C.** Area s32 has a striking layer II and a heavy SMI32-ir dendritic plexus. The black frame indicates the region of interest magnified in D. **D.** 1.5X magnification of layer II in NeuN and SMI32 preparations. Layer II is free of SMI32-ir and can thus be clearly differentiated from layer III. Reference to the adjacent and coregistered NeuN section shows that layer II of area s32 has a neuron dense superficial layer IIa and sparse layer IIb. Scale bar = 500 om.

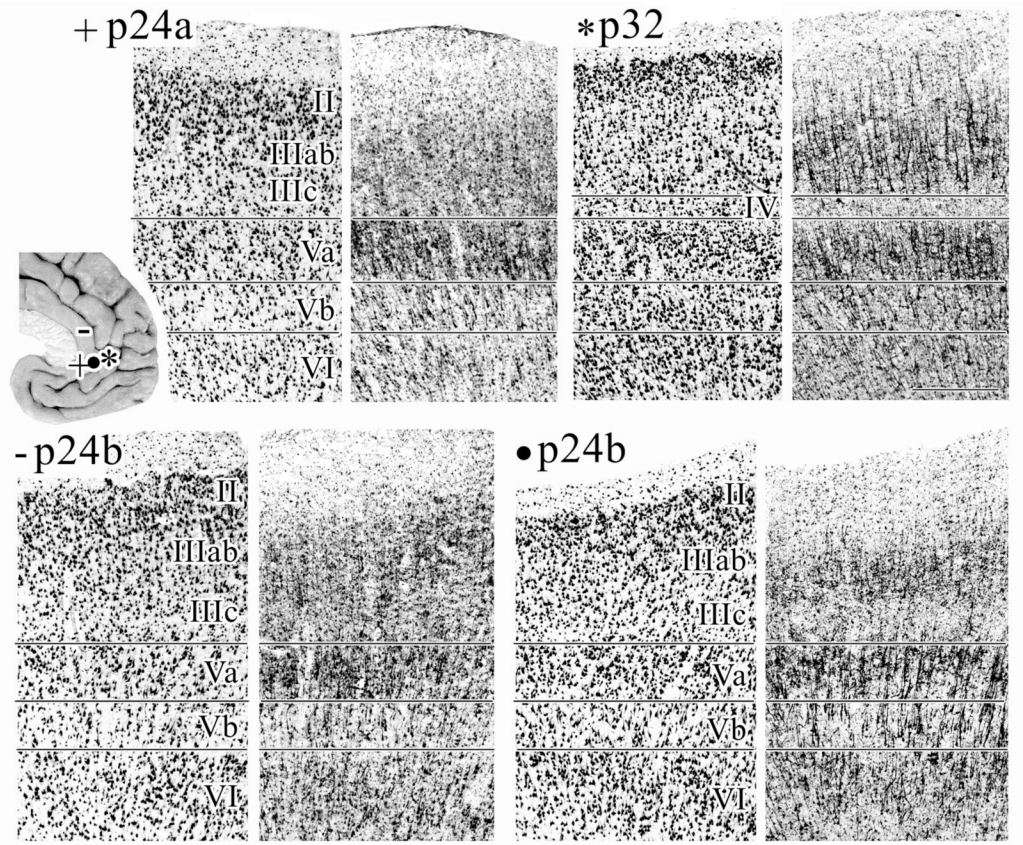

Figure 5.

Micrographs of areas s24a, s24b, and s32 taken from coronal sections immunoreacted for NeuN and SMI32. The locations at which micrographs were taken are marked by symbols on the inset brain. **Area p24a:** note the border between layers II–III of p24a is not visible in the silver-stained or NeuN sections, but can be shown by SMI32-ir. Layers of area p24a are generally wider than those of s24a (Fig. 4). **Area p24b** was photographed at two dorsoventral levels, emphasizing the lack of dorsoventral subdivisions within this area. Note, that layer II neurons merge almost indistinguishably into layer IIIab, and layer Vb contains many SMI32-ir neurons. **Area p32:** the deep layer III pyramids of area p32 are larger and more often SMI-ir when compared to those in s32. Scale bar = 500 om.

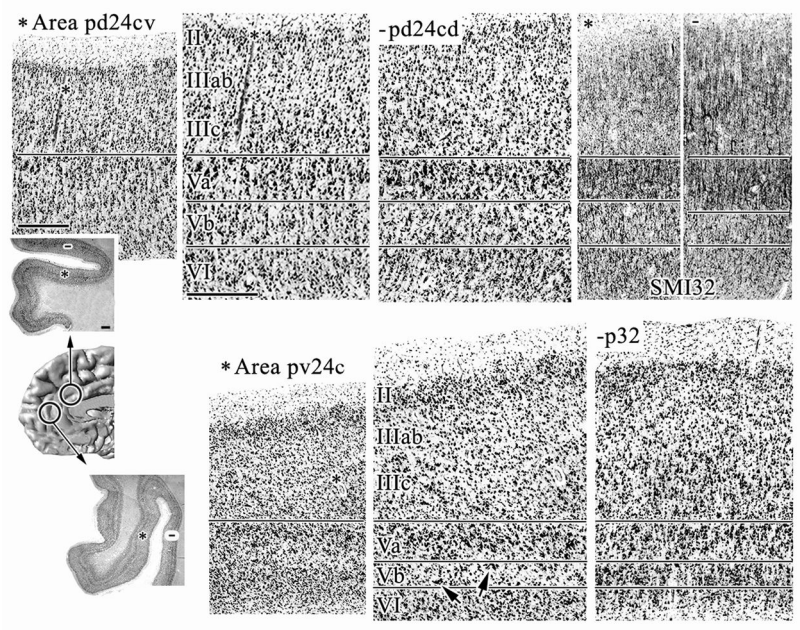

Figure 6.

Micrographs of area 24c taken at two dorsoventral levels as marked by circles on the medial surface of an MRI reconstructed human hemisphere. The top row of micrographs shows area pd24c and the bottom row shows pv24c. The two overviews are of coronal, silver cell-body stained sections and asterisks mark the position at which areas pd24cv and pv24cv were photographed. Asterisks in these micrographs mark blood vessels which serve as landmarks in both the lower (far left) and higher magnifications. Area pv24c has a broader and more dispersed layer II and neurons in layer Vb tend to form aggregates.

Hyphens in the overview sections mark the position at which areas pd24cd (top row) and p32 (bottom row) were photographed. Arrows highlight the cell clusters in layer Vb of area pv24cv. Micrographs of SMI32-ir were taken at comparable levels. When comparing areas pd24cv and pd24cd, note the higher densitiy of SMI32-ir fibers in layer III of area pd24cd as well as the higher number of large SMI32-positive pyramids which are not restricted to layer IIIc, but are also in layers IIIa–b. Scale bar in overview = 500 om; scale bar in micrographs = 500 om.

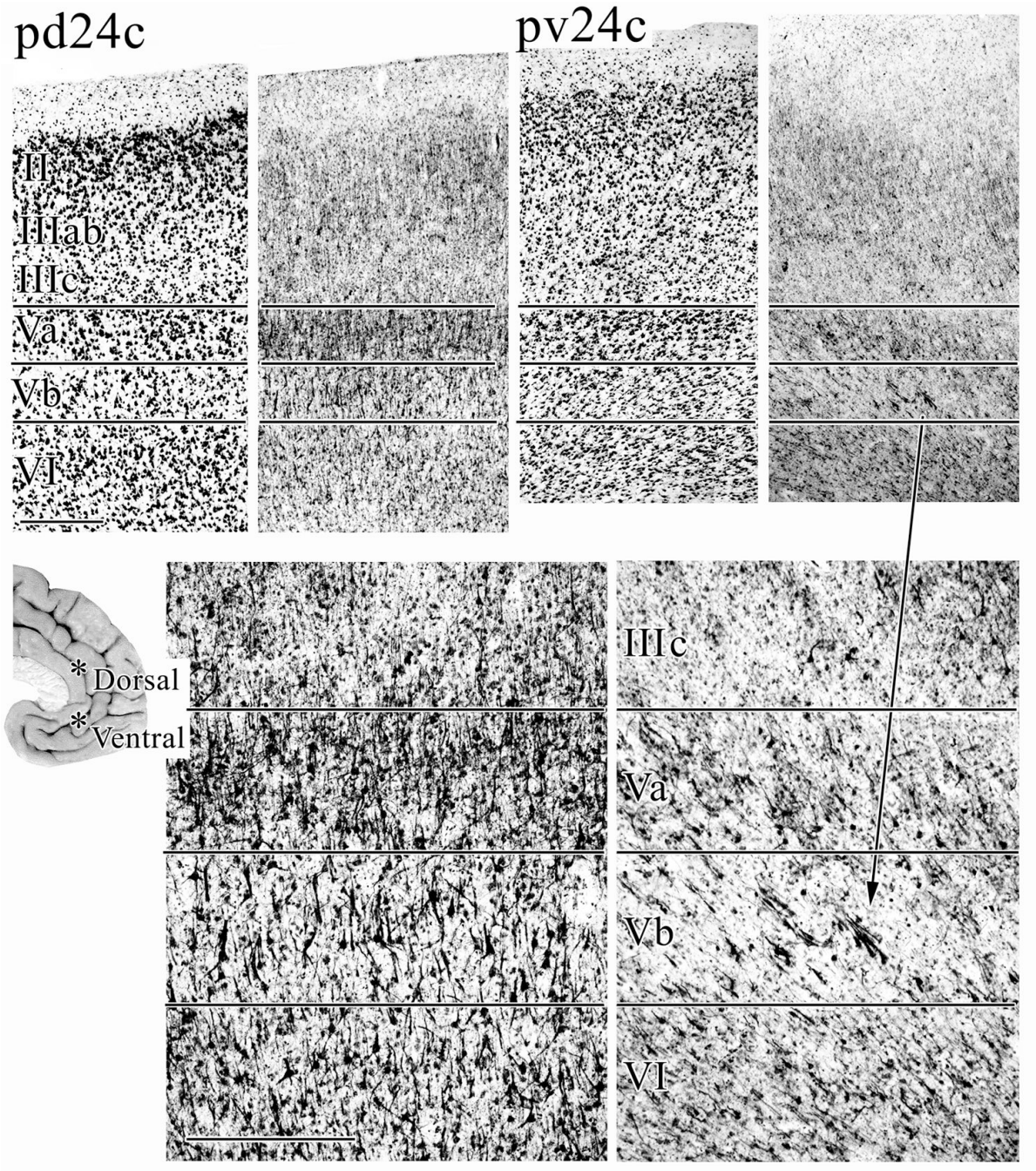

Figure 7.

Micrographs of coronal sections processed for NeuN and SMI32-ir showing the two dorsoventral components of area p24c (top row). Micrographs in the bottom row are a higher magnification of layers IIIc–VI from the SMI32 preparations. Area pd24c has a more prominent and SMI32-ir layer Va and a more densely packed layer Vb. The arrow points at the cell clusters in layer Vb of area pv24cv. Scale bar = 500 om.

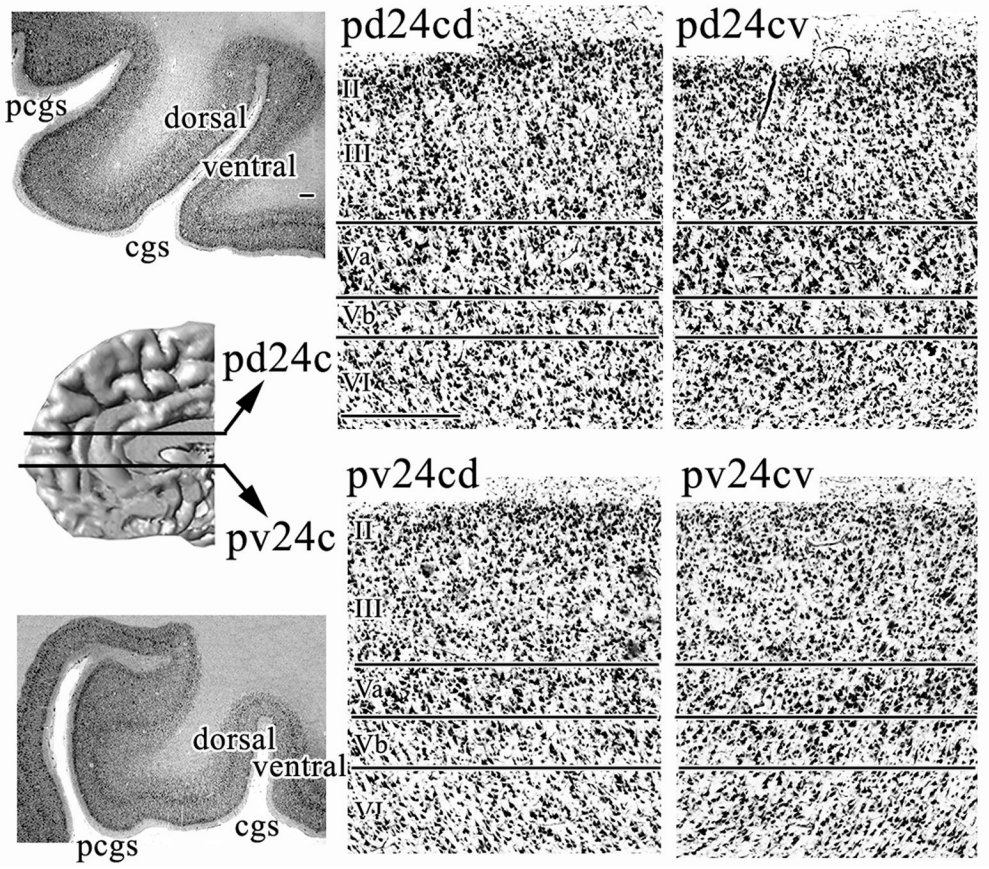

Figure 8.

Horizontal sections processed for silver cell-body staining through two dorsoventral levels of pACC. Area 24c was photographed on the dorsal (pd24cd and pv24c) and ventral (pd24cv and pv24c) banks of the cingulate sulcus at both locations. Note that the ventral section in this figure is located at a more dorsal position than the level at which area pv24cv was photographed in Figure 6. *cgs*: cingulate sulcus; *pcgs*: paracingulate sulcus. Scale bar in overview = 500 om; scale bar in micrographs = 500 om.

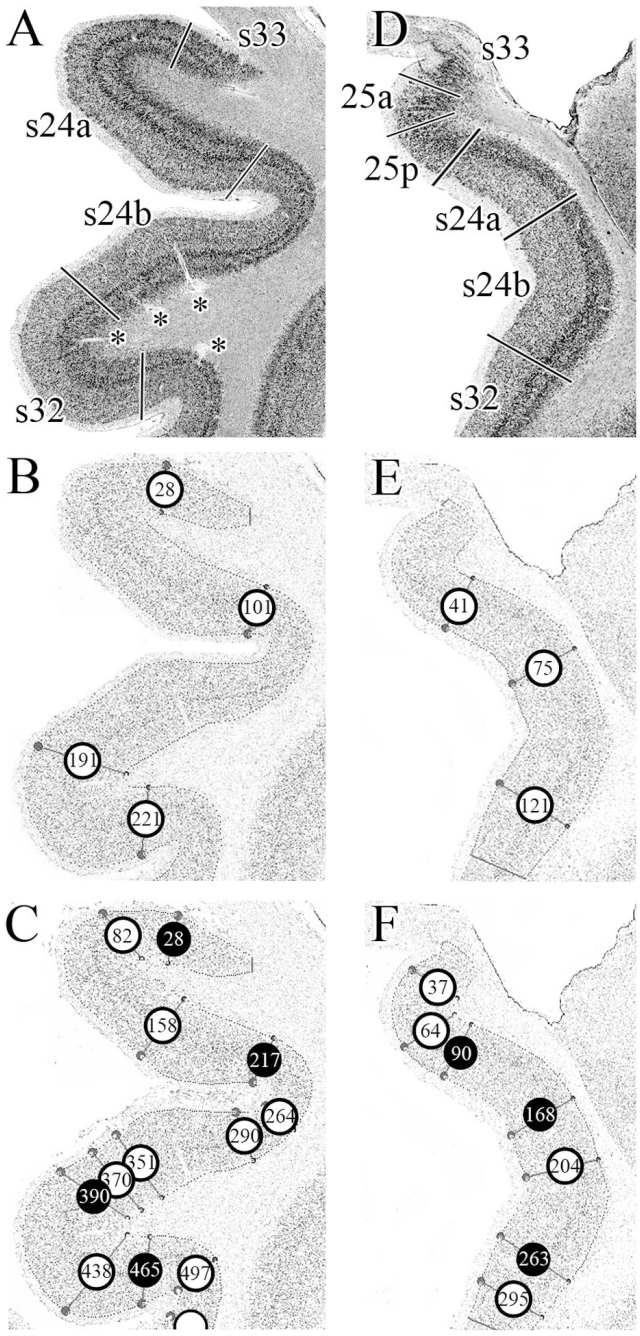

Figure 9.

Assessment of areal borders with an algorithm-based quantification of the cortical laminar pattern. **A.** Cell-body, silver stained coronal section through a rostral level of sACC with areas 33, s24a, s24b and s32. **B.** GLI-image of the section shown in A, where darker pixels code for higher GLI values and lighter pixels code for lower values. The cortex was sampled with equidistant traverses from layer II to the layerVI/white matter boundary. Traverses were extracted every 6 pixels. The start and end points of the traverses are indicated by the dots in the image at these two boundaries, but the traverses have been removed to simplify the figure. The algorithm-based quantification of the cortical laminar pattern is insensitive to artefacts such as blood vessels (marked by asterisks in A). Circles indicate borders detected by the sliding

window procedure at positions 28, 101, 191 and 221. **C.** GLI-image of the section shown in A, but traverses were extracted every 3 pixels (and not every 6 pixels, as in B). The sliding window procedure detected borders at positions 28, 82, 158, 217, 264, 290, 351, 370, 390, 438, 465, and 497. Black circles indicate the borders which coincide with the approach taken in B. **D.** Cell-body stained coronal section through a caudal level of sACC with areas 33, 25a, 25p, s24a, s24b, and s32. **E.** GLI-image of the section shown in D. Traverses were extracted every 6 pixels and the sliding window procedure detected borders at positions 41, 75 and 121. **F.** GLI-image of the section shown in A, but traverses were extracted every 3 pixels (and not every 6 pixels, as in E). The sliding window procedure detected borders at positions 37, 64, 90, 168, 204, 263, and 295. Black circles indicate the borders which coincide with the approach taken in E.

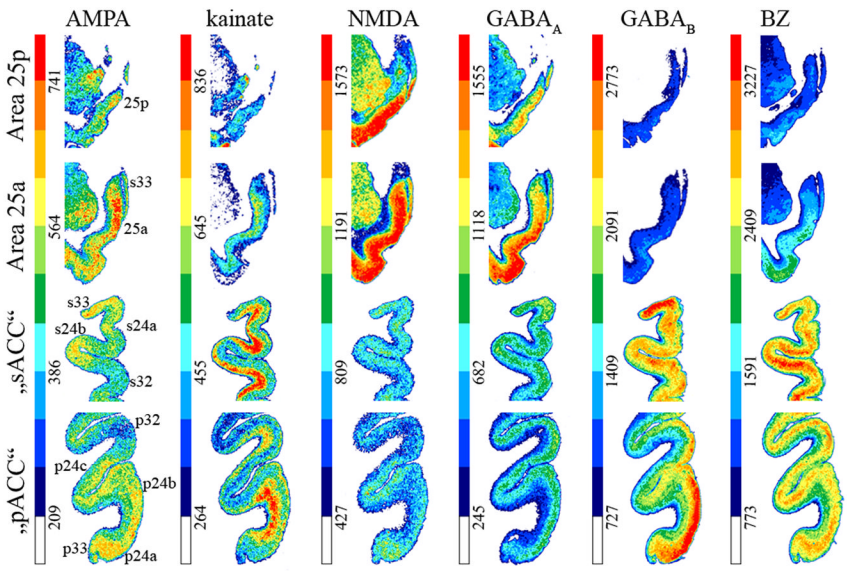

Figure 10.

Colour coded autoradiographs at different levels of ACC showing the distribution of receptors for glutamate (AMPA, kainate, NMDA) and GABA ($GABA_A$, $GABA_B$, $GABA_A$ associated benzodiazepine [BZ] binding sites). Scale bars code for receptor densities in fmol/mg protein.

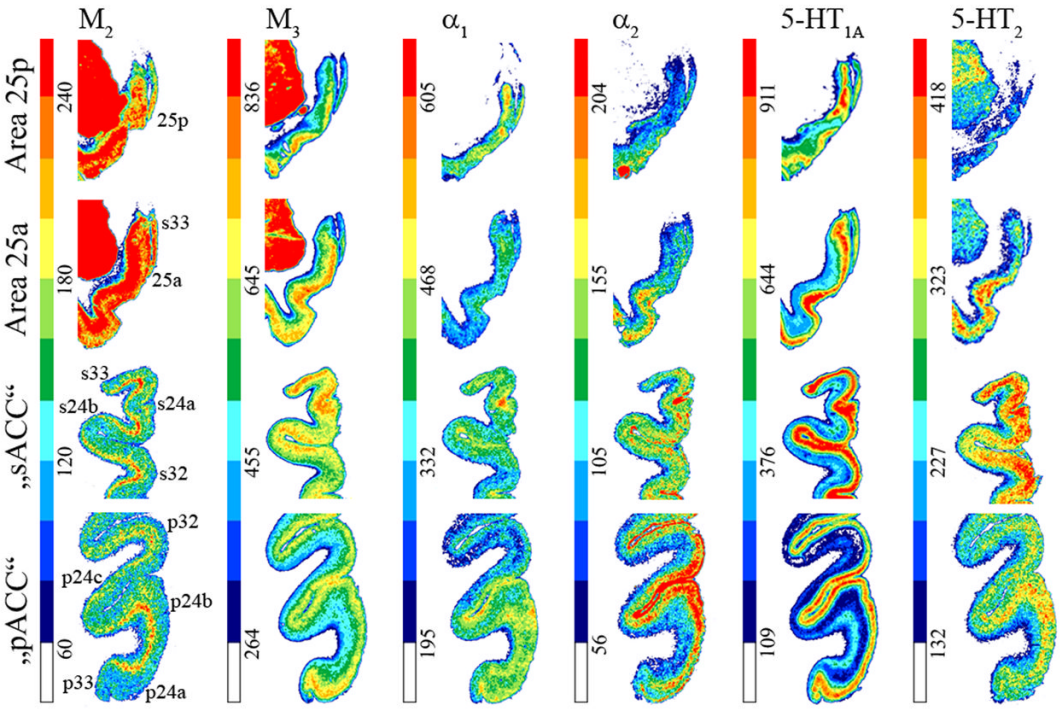

Figure 11.
Colour coded autoradiographs at different levels of ACC showing the distribution of receptors for acetylcholine (M_2, M_3), norepinephrine (α_1, α_2) and serotonin (5-HT_{1A}, 5-HT_2). Scale bars code for receptor densities in fmol/mg protein.

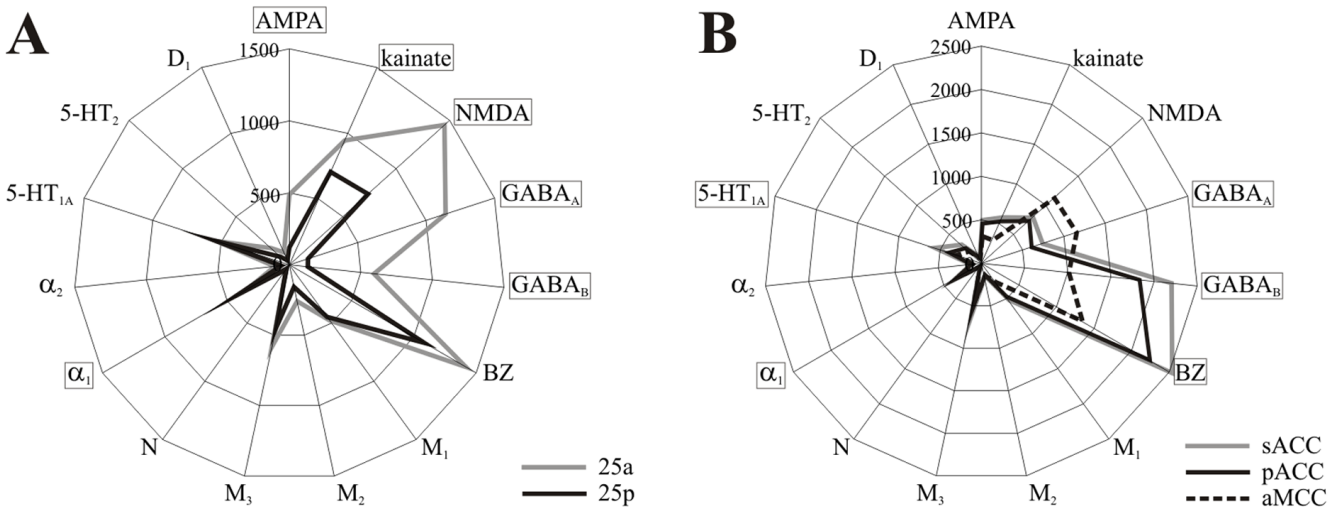

Figure 12.

Polar coordinate plots of ACC. **A.** Receptor fingerprints of sACC, pACC, and aMCC. Densities correspond to the average (in fmol/mg protein) of each receptor over all areas of a given region. Thus, sACC encompasses areas 25a, 25p, s33, s24a, s24b, and s32; pACC includes areas p33, p24a, p24b, pv24c, pd24c; aMCC comprises areas 33, a24a', a24b', a24c', and 32'. Densities range from 0 to 2500 fmol/mg protein, and receptors which were significantly different in sACC and pACC are highlighted. **B.** Receptor fingerprints of areas 25a and 25b. Densities range from 0 to 1500 fmol/mg protein, and receptors which were significantly different in 25a and 25p are highlighted.

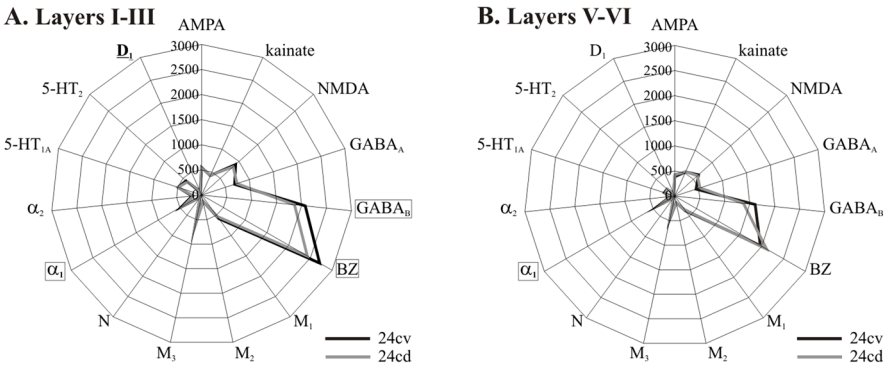

Figure 13.

A. Receptor fingerprints of the superficial layers of areas pd24cv and pd24cd. **B.** Receptor fingerprints of the deep layers of areas pd24cv and pd24cd. Receptor densities range from 0 to 3000 fmol/mg protein, and receptors which were significantly different in 24cv and 24cd are highlighted.

Table 1

Composition of stock solutions used for the silver cell body staining. Disolve components in the given order and stir thoroughly. Stock solutions can be stored for months at 4°C (stock solution A) or at room temperature (Stock solutions B and C).

	Stock solution A
000 |	distilled water
0	anhydrous sodium carbonate (Sigma- Aldrich)
	Stock solution B
000 |	distilled water
	ammonium nitrate (Merck)
	silver nitrate (Merck)
0	tungstosilicic acid hydrate (Fluka)
	Stock solution C
000 |	distilled water
	ammonium nitrate
	silver nitrate
0	tungstosilicic acid hydrate
.3 |	37% formaldehyde solution (Merck)

Table 2

Tritiated ligands used to label the examined receptors.

Neurotransmitter	Receptor	Ligand
Glutamate	AMPA	[^{3}H] AMPA
	kainate	[^{3}H] kainate
	NMDA	[^{3}H] MK-801
GABA	GABAA	[^{3}H] muscimol
	GABAB	[^{3}H] CGP-54626
	BZ	[^{3}H] flumazenil
Acetylcholine	M1	[^{3}H] pirenzepine
	M2	[^{3}H] oxotremorine-M
	M3	[^{3}H] 4-DAMP
	N	[^{3}H] epibatidine
Epinephrine	α_1	[^{3}H] prazosin
	α_2	[^{3}H] RX-821002
Serotonin	5-HT$_{1A}$	[^{3}H] 8-OH-DPAT
	5-HT$_2$	[^{3}H] ketanserin
Dopamine	D$_1$	[^{3}H] SCH-23390